REPORT DOCUMENTATION PAGE

Form Approved
OMB No. 0704-0188

1. AGENCY USE ONLY (Leave blank)	2. REPORT DATE	3. REPORT TYPE AND DATES COVERED
		FINAL

4. TITLE AND SUBTITLE
Low Threshold All-Optical Crossbar Switch on GaAs-GaAlAs Channel Waveguide Arrays

5. FUNDING NUMBERS
61102F
1602/01

6. AUTHOR(S)
Dr Tomasz Jannson

7. PERFORMING ORGANIZATION NAME(S) AND ADDRESS(ES)
Physical Optics Corporation
2545 West 237th Street, Suite
Torrence, CA 90505

8. PERFORMING ORGANIZATION REPORT NUMBER
AFOSR-TR- 95 0147

9. SPONSORING/MONITORING AGENCY NAME(S) AND ADDRESS(ES)
AFOSR/NE
110 Duncan Avenue Suite B115
Bolling AFB DC 20332-0001

10. SPONSORING/MONITORING AGENCY REPORT NUMBER
F49620-92-C-0047

11. SUPPLEMENTARY NOTES

12a. DISTRIBUTION/AVAILABILITY STATEMENT
APPROVED FOR PUBLIC RELEASE: DISTRIBUTION UNLIMITED

12b. DISTRIBUTION CODE

13. ABSTRACT *(Maximum 200 words)*

SEE FINAL REPORT ABSTRACT

14. SUBJECT TERMS

15. NUMBER OF PAGES

16. PRICE CODE

17. SECURITY CLASSIFICATION OF REPORT	18. SECURITY CLASSIFICATION OF THIS PAGE	19. SECURITY CLASSIFICATION OF ABSTRACT	20. LIMITATION OF ABSTRACT
UNCLASSIFIED	UNCLASSIFIED	UNCLASSIFIED	UNCLASSIFIED

GENERAL INSTRUCTIONS FOR COMPLETING SF 298

The Report Documentation Page (RDP) is used in announcing and cataloging reports. It is important that this information be consistent with the rest of the report, particularly the cover and title page. Instructions for filling in each block of the form follow. It is important to ***stay within the lines*** to meet ***optical scanning requirements***.

Block 1. Agency Use Only *(Leave blank)*.

Block 2. Report Date. Full publication date including day, month, and year, if available (e.g. 1 Jan 88). Must cite at least the year.

Block 3. Type of Report and Dates Covered. State whether report is interim, final, etc. If applicable, enter inclusive report dates (e.g. 10 Jun 87 - 30 Jun 88).

Block 4. Title and Subtitle. A title is taken from the part of the report that provides the most meaningful and complete information. When a report is prepared in more than one volume, repeat the primary title, add volume number, and include subtitle for the specific volume. On classified documents enter the title classification in parentheses.

Block 5. Funding Numbers. To include contract and grant numbers; may include program element number(s), project number(s), task number(s), and work unit number(s). Use the following labels:

C	- Contract	**PR**	- Project
G	- Grant	**TA**	- Task
PE	- Program Element	**WU**	- Work Unit Accession No.

Block 6. Author(s). Name(s) of person(s) responsible for writing the report, performing the research, or credited with the content of the report. If editor or compiler, this should follow the name(s).

Block 7. Performing Organization Name(s) and Address(es). Self-explanatory.

Block 8. Performing Organization Report Number. Enter the unique alphanumeric report number(s) assigned by the organization performing the report.

Block 9. Sponsoring/Monitoring Agency Name(s) and Address(es). Self-explanatory.

Block 10. Sponsoring/Monitoring Agency Report Number. *(If known)*

Block 11. Supplementary Notes. Enter information not included elsewhere such as: Prepared in cooperation with...; Trans. of...; To be published in.... When a report is revised, include a statement whether the new report supersedes or supplements the older report.

Block 12a. Distribution/Availability Statement. Denotes public availability or limitations. Cite any availability to the public. Enter additional limitations or special markings in all capitals (e.g. NOFORN, REL, ITAR).

- **DOD** - See DoDD 5230.24, "Distribution Statements on Technical Documents."
- **DOE** - See authorities.
- **NASA** - See Handbook NHB 2200.2.
- **NTIS** - Leave blank.

Block 12b. Distribution Code.

- **DOD** - Leave blank.
- **DOE** - Enter DOE distribution categories from the Standard Distribution for Unclassified Scientific and Technical Reports.
- **NASA** - Leave blank.
- **NTIS** - Leave blank.

Block 13. Abstract. Include a brief *(Maximum 200 words)* factual summary of the most significant information contained in the report.

Block 14. Subject Terms. Keywords or phrases identifying major subjects in the report.

Block 15. Number of Pages. Enter the total number of pages.

Block 16. Price Code. Enter appropriate price code *(NTIS only)*.

Blocks 17. - 19. Security Classifications. Self-explanatory. Enter U.S. Security Classification in accordance with U.S. Security Regulations (i.e., UNCLASSIFIED). If form contains classified information, stamp classification on the top and bottom of the page.

Block 20. Limitation of Abstract. This block must be completed to assign a limitation to the abstract. Enter either UL (unlimited) or SAR (same as report). An entry in this block is necessary if the abstract is to be limited. If blank, the abstract is assumed to be unlimited.

Research Sponsored by the Air Force Office of Scientific Research (AFMC)

Contract No.: F49620-92-C-0047

Low Threshold All-Optical Crossbar Switch on GaAs-GaAlAs Channel Waveguide Arrays

Final Report

Submitted to:

Contracting Officer
AFOSR/PK
Bolling AFB, DC 20332-6448

Contractor:

Physical Optics Corporation
Applied Technology Division
2545 West 237th Street, Suite B
Torrance, CA 90505

Principal Investigator:

Tomasz Jannson, Ph.D.
(310) 530-1416

September 14, 1994

REPORT D. CUMENTATION PAGE

Form Approved
OMB No. 0704-0188

1. AGENCY USE ONLY *(Leave blank)*	2. REPORT DATE	3. REPORT TYPE AND DATES COVERED
	September 14, 1994	Final, 7/15/92 to 7/14/94

4. TITLE AND SUBTITLE
Low Threshold All Optical Crossbar Switch on GaAs – GaAlAs Channel Waveguide Arrays

5. FUNDING NUMBERS
F49620-92-C-0047

6. AUTHOR(S)
Tomasz Jannson, Andrew Kostrzewski

7. PERFORMING ORGANIZATION NAME(S) AND ADDRESS(ES)
Physical Optics Corporation, Applied Technology Division
2545 West 237th Street, Suite B
Torrance, California 90505

8. PERFORMING ORGANIZATION REPORT NUMBER
3176

9. SPONSORING / MONITORING AGENCY NAME(S) AND ADDRESS(ES)
Contracting Officer
AFOSR/PK
Bollings AFB, DC 20332-6448

10. SPONSORING / MONITORING AGENCY REPORT NUMBER

11. SUPPLEMENTARY NOTES

12a. DISTRIBUTION / AVAILABILITY STATEMENT
Distribution Unlimited

12b. DISTRIBUTION CODE

13. ABSTRACT *(Maximum 200 words)*

During the Phase II project entitled "Low Threshold All-Optical Crossbar Switch on GaAs – GaAlAs Channel Waveguide Array," Physical Optics Corporation (POC) developed the basic principles for the fabrication of all-optical crossbar switches. Based on this development, POC fabricated a 2 x 2 GaAs/GaAlAs switch that changes the direction of incident light with minimum insertion loss and nonlinear distortion. This unique technology can be used in both analog and digital networks. The applications of this technology are widespread. Because the all-optical network does not have any speed limitations (RC time constant), POC's approach will be beneficial to SONET networks, phased array radar networks, very high speed oscilloscopes, all-optical networks, IR countermeasure systems, BER equipment, and the fast growing video conferencing network market. The novel all-optical crossbar switch developed in this program will solve interconnect problems, and will be a key component in the widely proposed all-optical 200 Gb/s SONET/ATM networks.

14. SUBJECT TERMS
Switch, CWA – Channel Waveguide Array, SNR – Signal-to-Noise Ratio

15. NUMBER OF PAGES
134

16. PRICE CODE

17. SECURITY CLASSIFICATION OF REPORT	18 SECURITY CLASSIFICATION OF THIS PAGE	19. SECURITY CLASSIFICATION OF ABSTRACT	20. LIMITATION OF ABSTRACT
Unclassified	Unclassified	Unclassified	SAR

TABLE OF CONTENTS

LIST OF FIGURES

LIST OF FIGURES (Cont)

LIST OF TABLES

1.0 INTRODUCTION

The connection and reconfiguration of a large number of information channels at very high modulation rates (> 10 Gb/s) according to a preset low is critical in the distribution of information within communication systems and optical neural networks. In order to provide this critical operation, in this program, Physical Optics Corporation (POC) developed an optically activated modulator (OAM) and a 10 x 10 GaAs channel waveguide array. These technologies can provide a number of practical applications that are critical to BMDO operations, such as high speed laser wavelength and incident direction sensors, GaAs-based IR countermeasure systems, variable fast switchable delay lines for microwave and MM wave phased arrays, optical gate generation of very short optical pulses, and time division multiplexing. In addition, the novel optical crossbar switch developed in this program solves the metrology problems related to analog and very high speed (> 15 Gb/s) digital bit error rate measurement techniques.

In this program, POC proposed a 10 × 10 all-optical crossbar switch based on an optically activated modulator/switch. In operation, a laser beam with an energy higher than the bandgap of the GaAs switches the propagation direction of the guided beam. Using this method, strong index modulation (>2%) that is not dependent on polarization for the EO effect can be induced. Both TE and TM guided waves have the same induced index change. The all-optic 10 x 10 switch uses a 0.8 μm pumping laser beam and a 1.3 μm probe beam. Because there are no electrical contacts, this all-optical switch has no RC time limits. Thus, the switching speed is limited only by the generated carrier lifetime, which is in the picosecond range. In order to optimize the switching efficiency, several optical switch designs were studied, including crossbar switches and directional coupler switches. To realize multichannel optical switches, a compact self-aligned packaging technique was developed.

Over the course of the Phase II project, we realized the need for a efficient software simulation tool to enhance our waveguide design capabilities. Our search for a commercial software was unsuccessful, so we decided to develop our own, with the goal of making it commercially available in the near future. After several months of development, we created a flexible Microsoft Windows™ compatible software package that can be used in a variety of waveguide design tasks, and offers a wide range of material choices and waveguide geometries. The software is fully operational, and POC is planning to make it commercially available later this year.

The software has been fully tested in this program, and was used to design a waveguide array with minimum crosstalk between channels and low absorption. The importance of the waveguide design software is especially amplified in the case of waveguide arrays and waveguide switches.

1.1 The Highlights of Phase II Project Findings and Achievements

During the course of Phase II, POC developed a low threshold 10x10 GaAs all-optical crossbar switch. The major highlights and achievements of Phase II are:

1. POC calculated the optical waveguide dimensions, and waveguide propagation loss. Based on this calculation, the configuration of the optical crossbar switch can be designed using standard CAD programs.

2. POC fabricated a 2x2 GaAs switch that changed direction of analog NTSC video signals. This crossbar switch has been demonstrated and laboratory tested.

3. POC designed multiple masks for the multilayer switch structure, and investigated different types of etching materials to reduce waveguide insertion loss and minimize crosstalk.

4. POC tested the 2x2 GaAs crossbar switch and determined its insertion loss, crosstalk between separate channels, optical activation, and coupling loss.

5. POC evaluated the power budget of the optical crossbar switch, and provided BER measurements using POC's unique BER measurement technique. This enabled us to evaluate the crosstalk and insertion loss of the system, which is important for very high speed SONET networks.

6. POC determined the potential uses for the new optical crossbar switch. These uses include incident direction sensors, optical switches, full optical BER testers, IR countermeasure systems, and variable delay lines for MMW phased radar arrays. The applications for POC's novel technology are widespread.

2.0 THE MODELING OF HIGHLY PARALLEL SINGLEMODE CHANNEL WAVEGUIDE ARRAY

Interconnection length and packaging density are important parameters in a 10 x 10 crossbar switch. The replacement of electrical interconnects with optical interconnects requires a medium in which optical signals can be routed from the transmitters to the receivers. For this purpose, two available choices are optical fibers and thin film waveguides. For machine-to-machine optical interconnects, optical fibers are the medium of choice. For interconnection scenarios such as crossbar switches, backplanes, intermodular, and intramodular, thin film channel waveguides are the major tools under intensive investigation [1-5]. In addition, thin film channel waveguide arrays are important building blocks for many optoelectronic interconnection systems [6-9], since they are the only guided-wave interconnection devices that can be lithographically mass produced.

The two key criteria that determine the usefulness of such interconnects are the interconnect length and packaging density. The channel length and density of waveguide arrays may be limited for many reasons, including propagation losses and crosstalk caused by stray light from scattering, reflection, and diffraction. It has been reported [10,11] that the crosstalk between neighboring

waveguides must be smaller than -12 dB for incoherent light sources, and -32 dB for coherent lights sources. Based on our analysis and experimental results, the coupling-induced crosstalk between channel waveguides gives rise to major limitations in both interconnection length and packaging density of a singlemode channel waveguide array (SMCWA). In an optical interconnect system using a GaAs-GaAlAs SMCWA with a refractive index $n_1 = 3.4$ and a lateral index difference $\Delta n = (n_1 - n_{3.5})/n_1 = 0.001 \sim 2.4$ (see Figure 2-1), our results indicate that the channel separation must be larger than two channel dimensions, in the range of 2 to 7, in order to provide the required signal-to-noise ratio.

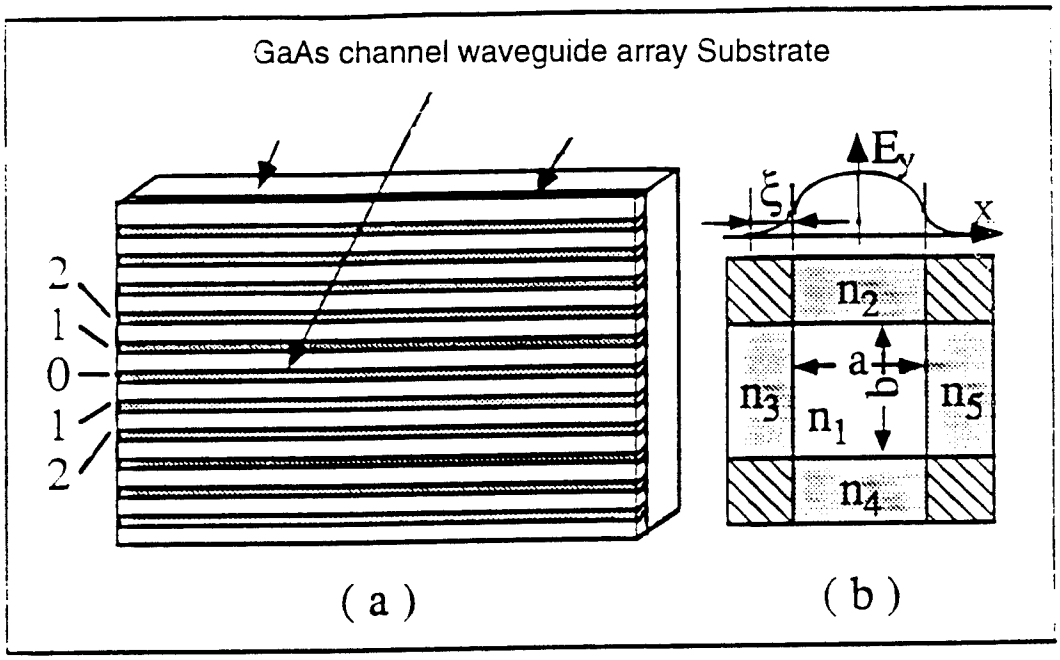

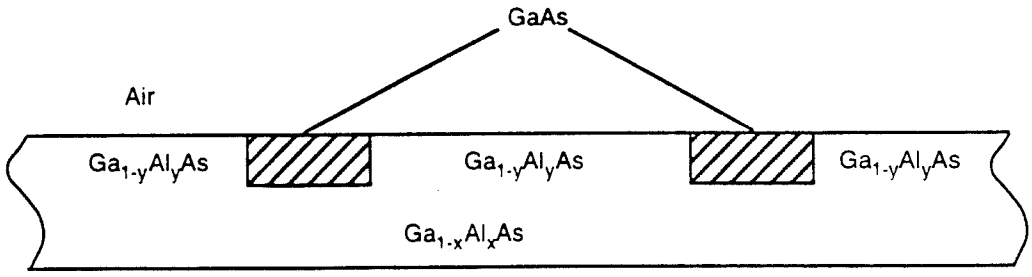

(c)

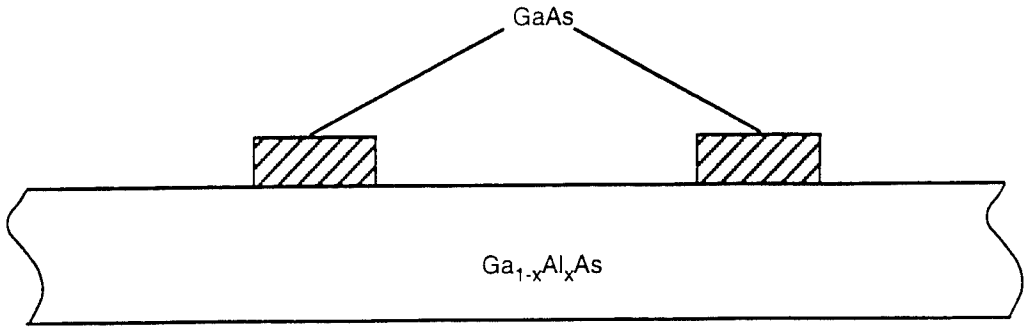

(d)

Figure 2-1
(a) A Schematic Diagram of a GaAs Channel Waveguide Array. (b) The Cross Section of a Channel Waveguide Under Consideration. Here, all calculations are conducted with a = b. (c) The creation of the lateral index difference ($n_1 - n_{3,5}$) between GaAs and GaAlAs heterostructures. (d) The vertical index (n_1 - ny) causes a difference in the refractive index between GaAs and Ga_{1-x} Al_xAs.

Here, we assume a cross-talk model that considers cross-coupling between an infinite number of parallel waveguides. This model relates the maximum interconnect length and packaging density to the waveguide parameters of an SMCWA. The trade-off between minimum channel separation (MCS) and maximum channel length (MCL) is determined with the crosstalk noise as a parameter. This noise is generated by the cross-coupling between the light waves propagating in different channel waveguides [12-14]. Our crosstalk model yields an optimum design to obtain a high packaging density and long interconnection lengths. The effects of the coherence of the light source on MCS and MCL are discussed for both multiple channel cross-coupling and receiver phase-to-intensity noise conversion mechanisms. Using a GaAs – GaAlAs SMCWA [3-5], the channel packaging density limitations caused by channel cross-coupling were experimentally observed and studied, confirming our theory presented herein.

2.1 The Optimization of Waveguide Dimensions

In the following analysis, we consider an optical interconnection system using identical singlemode channel waveguides with uniform channel separation. For simplicity, the symmetric singlemode channel waveguide is selected with a channel width a equal to b, and $n_1 > n_2, n_3, n_4, n_5$. Here, n_1 and n_{2-5} are the refractive indices of the guiding layer and cladding layers, respectively. Figure 2-1(a) shows a schematic diagram of a linear channel waveguide array on GaAs. The cross section of a channel waveguide is depicted in Figure 2-1(b) for theoretical modeling simplicity. The lateral index difference (n_1-$n_{3,5}$) is created by the GaAs and GaAlAs heterostructure (see Figure 2-1(c)), or etching (see Figure 2-1(d)). The vertical index difference (n_1-n_4) is due to the difference in the refractive indices of GaAs and $Ga_{1-x}Al_xAs$. The equations used to determine the refractive index of GaAs and GaAlAs are given by the Sellmeier equation

$$n^2 = A(x) + \frac{\beta}{\lambda^2 - C(x)} - D(x)\lambda^2 \qquad (2\text{-}1)$$

where x is the mole percent of aluminum, and λ is the light wavelength in free space. The Sellmeier equation coefficients A, B, C, and D are given in Table 2-1.

Table 2-1. Sellmeimer Equation Coefficients (λ is μm)

Material	A	B	C	D
GaAs	10,906	0.97501	0.27969	0.00246
$Ga_{1-x}Al_xAs$	10,906 -292x	0.97501	(0.52886 -0.735x)^2 for $x \leq 0.36$ (0.30386 -0.105x)^2 for $x>0.36$	0.00246 (1.41 x + 1)

At λ = 1.3 μm and n_1 = 3.4, we assume that n_2 = 1.0 for air. The dimensions of a singlemode channel waveguide are dependent not only on the refractive indices of the guiding medium and cladding layers, but also on the operating wavelength [30]. As the optical wavelength becomes shorter and the relative index difference $\Delta n = (n_1 - n_{3,4,5})/n_1$ increases, singlemode waveguide dimensions shrink. However, practical considerations limit the miniaturization of waveguides. For example, it is very difficult to achieve efficient coupling between a light source and a channel waveguide with a cross section smaller than the beam width of the TEM_{00} mode of a laser. Singlemode channel waveguides with dimensions close to the cutoff boundary of the second mode are preferred for high packaging density in a CWA design. The required waveguide dimensions can be calculated after the relative index difference has been determined. Note that the channel density is determined by the sum of the channel width and channel separation.

For the SMCWA shown in Figure 2-1, the optical wave propagating though each channel waveguide may couple out to adjacent channels. In many cases, this effect results in a major limitation on minimum channel separation (MCS) and maximum channel length (MCL). The coupling coefficient between two fundamental TE waves propagating through two neighboring singlemode channel waveguides can be approximated as [12],

$$|K| = \frac{1}{a\xi k_z} \exp(-c/\xi) \qquad (2\text{-}2)$$

where $k_z = (2\pi n_1/\lambda - 2/\xi)$ for a symmetric square channel waveguide, λ is the operating wavelength, c is the channel separation, and $\xi = \xi 3 = \xi 5$ represent the penetration depths of the field components in cladding media 3 and 5. For singlemode operation, ξ is given by

$$\xi = \frac{A}{\pi}\left\{1 - \left[\frac{A}{a}\,\frac{1}{1+\frac{2A}{\pi a}}\right]^2\right\}^{-0.5} \tag{2-3}$$

where $A = \frac{\lambda}{2}\left(n_1{}^2 - n_{3,5}{}^2\right)^{-0.5}$. Note that ξ is primarily determined by a, n_1, n_3 and n_5, rather than by b, n_2 and n_4.

Thus,

$$I_{coh} = \left\{2\sin(|K|z) + 2\sin^2(|K|z) + \sin^3(|K|z)\ldots + 2\sin^n(|K|z)\right\}^2 \tag{2-4}$$

and

$$I_{inc} = 2\left\{\sin^2(|K|z) + \sin^4(|K|z) + \sin^6(|K|z)\ldots + \sin^{2n}(|K|z)\right\} \tag{2-5}$$

for coherent and incoherent light, respectively. 2n+1 is the total number of waveguides. In Eqs. (2-4) and (2-5), z is the coupling length; i.e., the length of the channel waveguide. Note that coherent light sources are defined as sources whose linewidths (Δv) and inter-source frequency spacing are much smaller than the electrical bandwidth of the receiver [11]. Eqs. (2-4) and (2-5) were obtained by assuming that: 1) the guided waves propagating in each channel could couple into the center channel through adjacent channels; and 2) all guided waves coupled into the center channel were in phase and would not couple back to other channels.

These assumptions represent the worst case condition for crosstalk, and thus impose the most stringent conditions for the design of a CWA. Propagation losses are neglected in Eqs. (2-4) and (2-5), because they do not contribute to crosstalk.

For coupling conditions where $|K|z << 1$ and $n \rightarrow \infty$, Eqs. (2-4) and (2-5) can be written as

$$I_{coh} = 4\left[\frac{|K|z}{1-|K|z}\right]^2 \quad \text{and} \tag{2-6}$$

$$I_{inc} = 2\frac{\left[|K|z\right]^2}{\left[1-|K|z\right]^2} \tag{2-7}$$

Eqs. (2-6) and (2-7) indicate that the optical intensity coupled into the center channel from other channels is a function of the coupling coefficient and channel length. By substituting Eq. (2-2) into Eqs. (2-6) and (2-7), the minimum channel separation can be obtained as

$$c_{coh} = -\xi \ln\left[\frac{a\xi k_z}{z}\frac{2(I_{coh})^{0.5} - I_{coh}}{(4 - I_{coh})}\right] \text{ and} \tag{2-8}$$

$$c_{inc} = -\xi \ln\left[\frac{a\xi k_z}{z}\left(\frac{I_{inc}}{2 + I_{inc}}\right)^{0.5}\right]. \tag{2-9}$$

Eqs. (2-8) and (2-9) are very useful in designing SMCWAs. If all of the parameters of a SMCWA are known, including waveguide indices, dimensions, and signal wavelength, the minimum channel separation can be obtained by setting a desired crosstalk noise criterion, I_{coh} and I_{inc}.

The crosstalk noise criteria, I_{coh} and I_{inc}, can be determined based on system performance from the SNR required at the output end of a SMCWA, defined as $R = 10 \log_{10}\left[\frac{I_s}{I_n}\right]$. In our case, using normalized intensity, we have $I_s = 1$ and $I_n = I_{coh}$ or $I_n = I_{inc}$, which are given by Eqs. (2-3) and (2-4), respectively. If binary pulse code modulation is employed in an optical interconnection network, the SNR must be large enough to obtain the required bit error rate. At a BER of 10^{-15}, the required SNR is 12 dB for incoherent light sources, and 32 dB for coherent light sources, assuming an extinction ratio of 20, a laser linewidth of 2 GHz, an electrical bandwidth of 10 GHz, and a 1 dB power penalty criterion. The 20 dB difference in the required SNR between coherent and incoherent light sources is due to the effects of phase-to-intensity noise conversion in avalanche photodiodes. This difference varies with the degree of coherence $\left(\frac{BW}{\Delta v}\right)$, and saturates at ~20 dB [10, 11].

The minimum channel separation versus the SNR based on Eqs. (2-7) and (2-8) is plotted in Figure 2-2. Two symmetric square SMCWAs were selected with channel widths of 3 μm and 10 μm, and relative index differences (Δn) of 0.01 and 0.001, respectively. As indicated in Figure 2-2, the coherence of the light source results in a different minimum channel separation. Furthermore, because the SNR imposed by an optical interconnect system using a coherent light source is much higher than that of a system using an incoherent light source, the minimum channel separation may vary by up to a few channel widths if optical waves with different degrees of temporal coherence are employed. For example, using a 1 dB power penalty criterion at a BER of 10^{-15}, the SNR needed at the output end of the SMCWA is 12 dB for incoherent light and 32 dB for coherent light, as shown in Figure 2-2.

Figure 2-2 also indicates that different waveguide dimensions, corresponding to different Δn values, should require different channel separations to ensure a desired SNR. Based on this data,

the optimum waveguide packaging densities were found to be in the range of 225-550 channels/cm for coherent light sources, and 300-700 channels/cm for incoherent light sources.

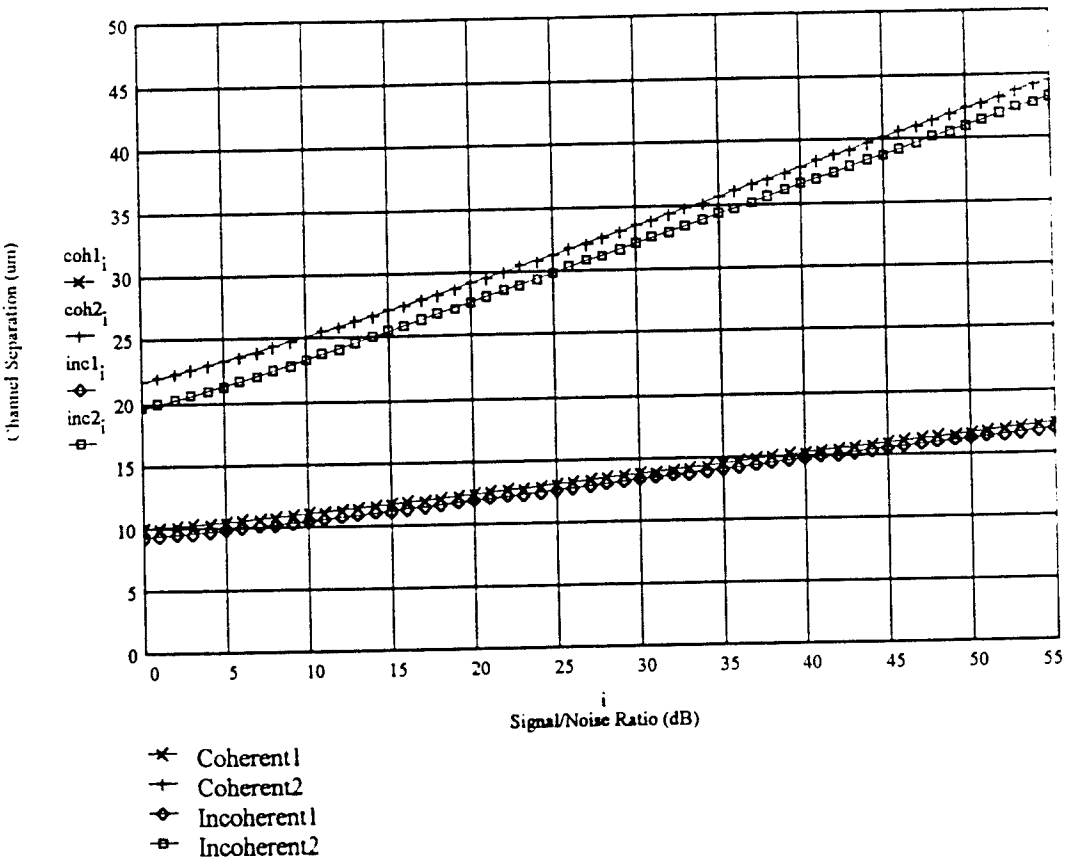

Figure 2-2
Minimum Channel Separation Versus Signal/Noise Ratio Based on Equations 2-7 and 2-8. $z = 2$ cm, $n_1 = 1.5$, $n_2 = 1.0$. $\Delta n = 0.01$ for $a = 3$ μm and $\Delta n = 0.001$ for $a = 10$ μm at $\lambda = 1.5$ μm were assumed.

In order to find the optimum design rule, the minimum channel separation versus waveguide dimension in a SMCWA was determined based on Eqs. (2-7) and (2-8), and is plotted in Figure 2-3. The relationship between MCS and penetration depth is also shown in this figure, with channel widths ranging from 1.75 μm to 5.5 μm for singlemode operation. Minimizing the evanescent tail, and thus maximizing the confinement factor, plays a paramount role in high packaging density channel waveguide arrays. Note that this interesting result is pivotal in designing waveguide-grating wavelength routers, where high packaging density, long channel lengths, and large waveguide dimensions are all necessary [9]. The physical parameters of the symmetric square SMCWA used in these calculations can be found in Figure 2-3.

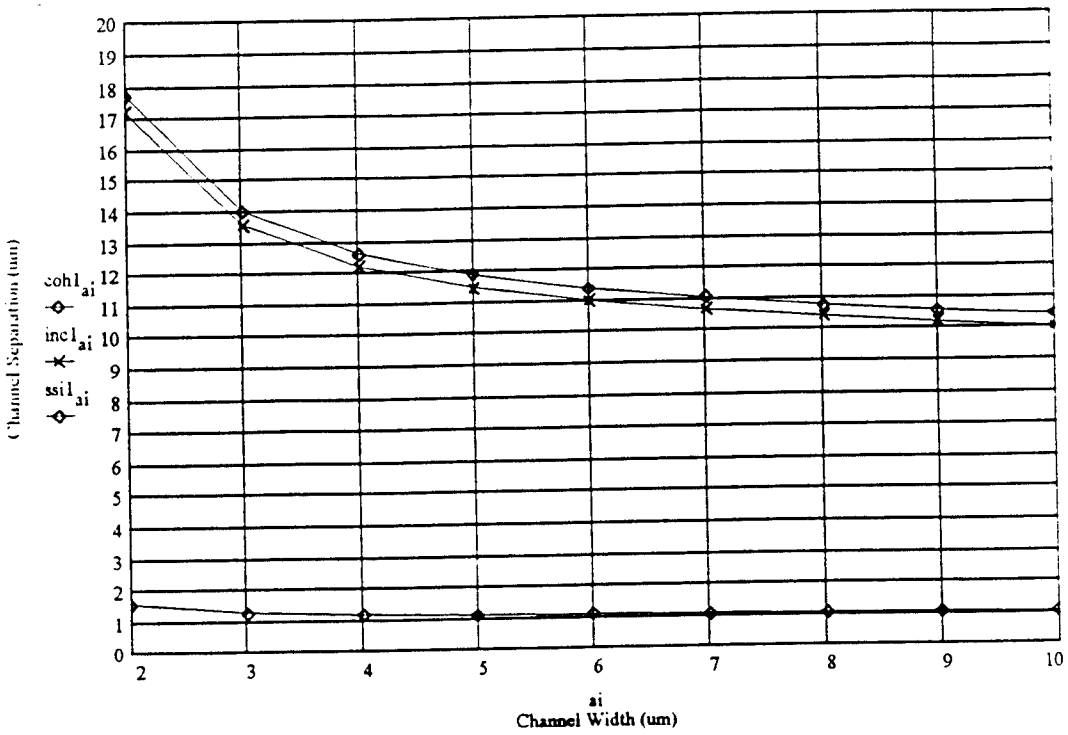

Figure 2-3
Minimum Channel Separation Versus Channel Width to Ensure a Minimum of 32 dB Signal/Noise Ratio. The penetration depth ξ is also shown in the figure. $z = 2$ cm, $n_1 = 1.5$, $n_2 = 1.0$, and $\Delta n = 0.01$ at $\lambda = 1.3$ µm were assumed.

The packaging density of the SMCWA with a given cross-talk figure is primarily determined by the index difference between the waveguide guiding layer and cladding layer; the larger the relative index difference, the smaller the channel separation will be. The minimum channel separation versus the relative index difference, based on Eqs. (2-7) and (2-8), is plotted in Figure 2-4. As indicated in this figure, a large relative refractive index is preferred to obtain densely packed SMCWAs. The relationship between minimum channel separation (MCS) and penetration depth is also shown in this figure, with Δn ranging from 0.003 to 0.013 for singlemode operations. However, if the refractive index difference is too high, the dimensions of a singlemode channel waveguide will be very small, (close to 2 µm for $\Delta n = 0.3$ and a = 10 cm), which can create light source-to-waveguide coupling difficulties. The physical parameters of the symmetric square SMCWA used in the calculation can be found in Figure 2-4.

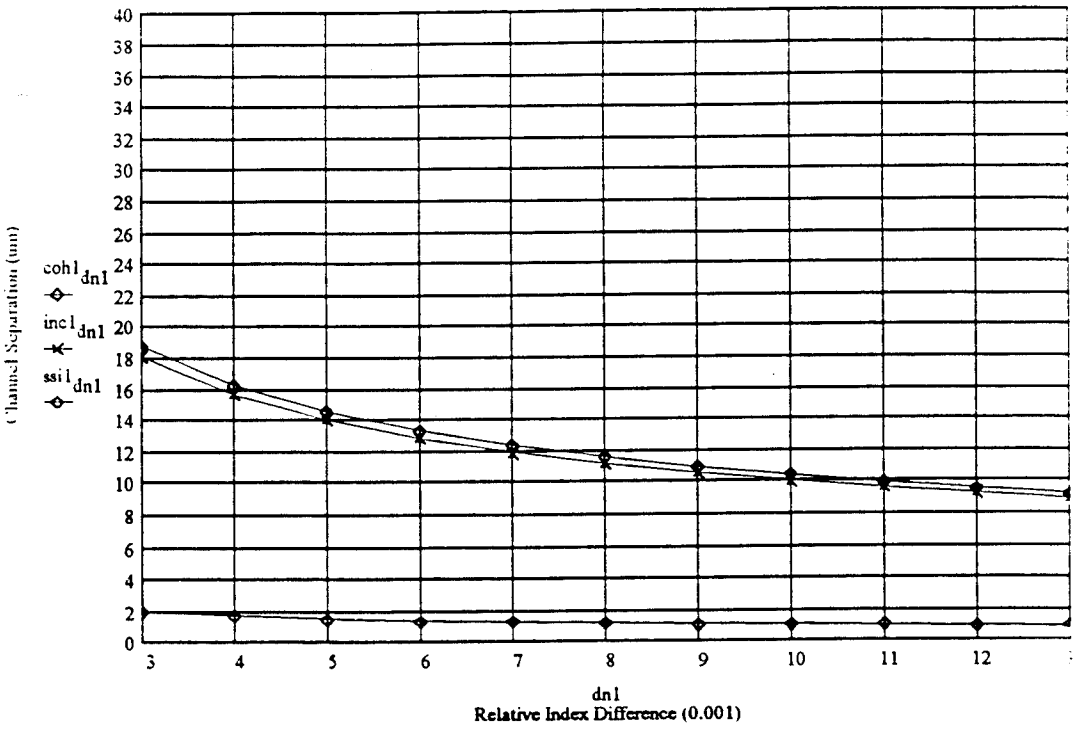

(a)

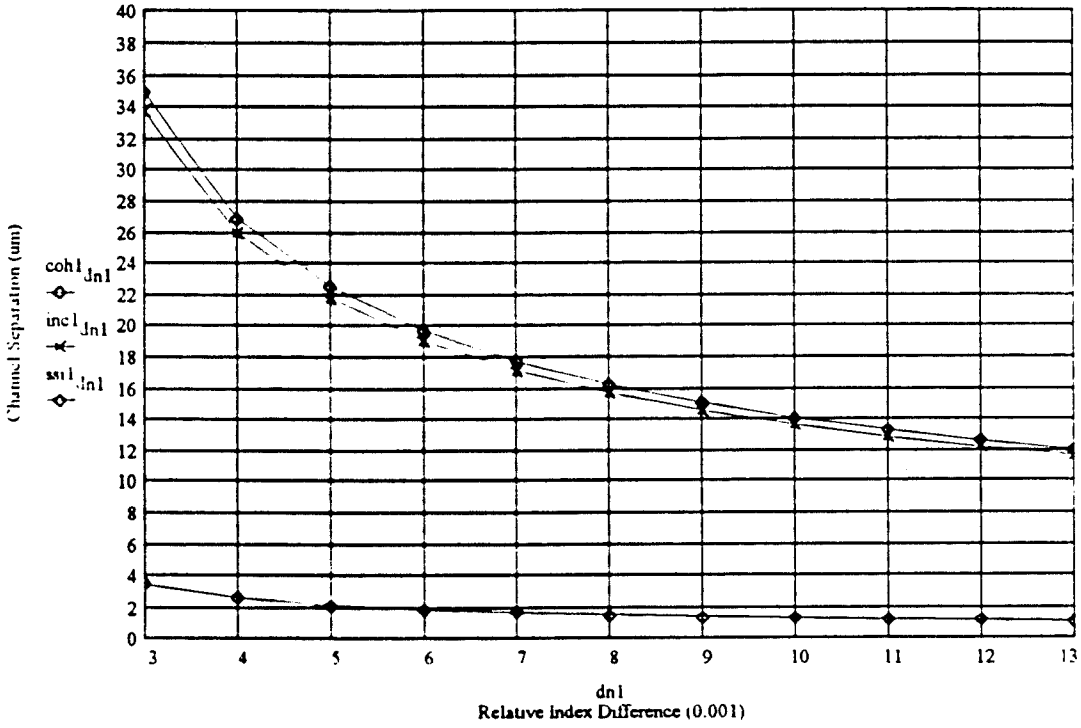

(b)

Figure 2-4
Minimum Channel Separation Versus Relative Index Difference to Ensure a Minimum of 32 dB SNR Based on Eqs. (2-7) and (2-8). The penetration depth is also shown in the figure. $z = 2$ cm, $n_1 = 1.5$, $n_2 = 1.0$, and $\Delta n = 0.01$ at $\Delta n = 0.01$ at $x = 1.3$ μm were assumed with $a = 10$ μm for (a) and $a = 3$ μm for (b)

If all related waveguide parameters are defined, Eqs. (2-8) and (2-9) can be used to derive the maximum channel length and packing density:

$$z_{coh} = a\xi k_z \left[\frac{2(I_{coh})^{0.5} - I_{coh}}{4 - I_{coh}} \right] \exp\left(\frac{c}{\xi} \right) \tag{2-10}$$

and

$$z_{inc} = a\xi k_z \left[\frac{I_{inc}}{2 + I_{inc}} \right]^{0.5} \exp\left(\frac{c}{\xi} \right) \tag{2-11}$$

These two equations indicate that the channel length increases exponentially with the channel separation for a fixed Δn. The longer the channel length, the larger the channel separations must be in order to ensure a desired SNR. This demonstrates the tradeoff between channel packaging density and interconnect length.

The relationship between the maximum channel length and the minimum channel separation is expressed by Eqs. (2-10) and (2-11), which show that the maximum channel length is strongly affected by channel separation in a dense SMCWA. There is a threshold value for channel separation that is required in order to obtain an optimized optical interconnection length using a SMCWA. Larger waveguide dimensions, corresponding to a smaller Δn, give rise to a higher threshold values for channel separation. In order to obtain the required optical interconnection length with $a = 3\ \mu m$ and $\Delta n = 0.01$, and $a = 10\ \mu m$ and $\Delta n = 0.001$ (at $n_1 = 1.5$), it would be necessary to separate the waveguides at least 3 times the channel width. Waveguide separation can be about 2 times the channel width if we increase Δn by etching isolation slots between channels. In a dense SMCWA, there is a significant difference between the maximum interconnection lengths of systems employing coherent and incoherent light sources. In spite of the limitations caused by the cross-coupling between channel waveguides, very long interconnecting lengths (~50 cm) with high packaging density (~650 channel/cm) can be achieved by employing GaAs SMCWAs.

2.2 Experimental Results for Waveguide Array

To verify the packaging density limitations caused by channel cross-coupling in a dense SMCWA, a SMCWA on GaAs was fabricated and tested. The fabricated SMCWA had a uniform channel separation of 8 μm, a channel width of 2 μm, and a channel length of 2 cm. $n_1 = 1.5$, ($n_2 = 1.0$), $\Delta n = 0.004$, $n1\text{-}n_4 \approx 0.01$ and propagation losses of about 0.1 dB/cm were experimentally determined [3,15]. An InGaAs laser with uniform intensity operating at a wavelength of 1.3 μm was coupled into the SMCWA. Because of channel cross-coupling, significant optical power was transferred among the waveguides, resulting in a non-uniform intensity distribution at the output

end of the SMCWA. Such effects give rise to undesired optical crosstalk, which can set major limitations on system performance.

To further identify and evaluate multiple channel cross-coupling in this experiment, three optical beams from a HeNe laser (λ = 1.3 μm) with uniform intensity were coupled into the three center waveguides of the array. No optical power was launched into any of the other channels at the array input. Figure 2-5 is the image of mode profile of each channel obtained at the output end. The cross-coupling among 5 channels is clearly shown in the figure. As indicated in Figure 2-6, significant optical power (up to 20%) was transferred into the outer channels and the center channel at the output end of the channel waveguide array. Figures 2-6(a) and 2-6(b) are plots of the calculated intensity distribution in a SMCWA, where three input light waves with the same intensity were assumed at the input ends of the three center channels. This calculation assumes z = 2 cm, n_1 = 1.5, Δn = 0.004, a 2 μm, and c = 8 μm. The optical intensity in each channel waveguide is further assumed to have Gaussian distribution with a beam waist w = (a + ξ). The agreement between Figures 2-5 and 2-6 is obvious. Note that Figure 2-6 was obtained by modifying Eq. (2-3) on each channel while considering the energy conservation among all the channels.

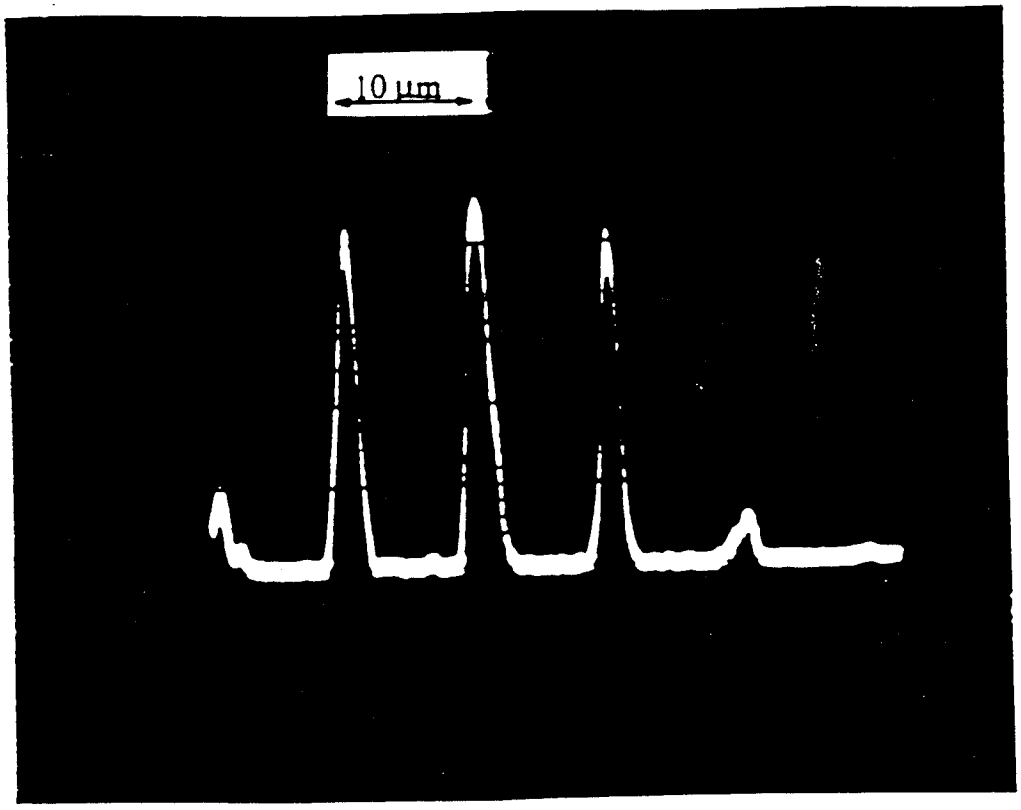

Figure 2-5
Photograph of Experimental Result for Multiple Channel Cross-Coupling (n = 3) in a Polymer Based SMCWA with n_1 = 1.5, n_2 =1.0, Δn = 0.004, a = 2 μm, c =8 μm, and z = 2 cm at λ = 1.3 μm.

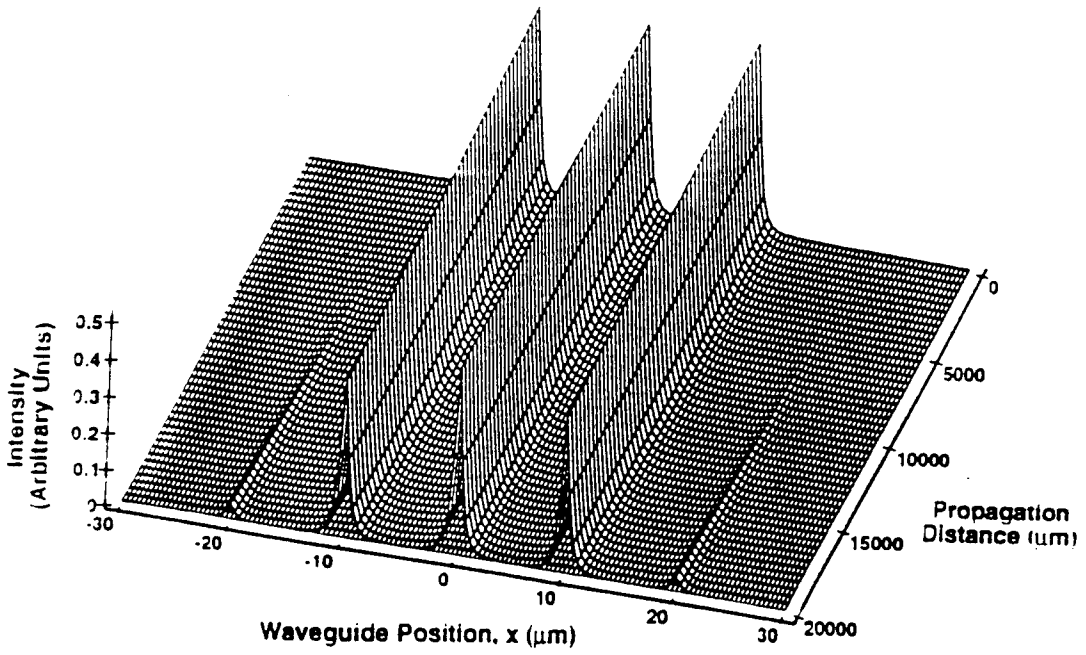

Figure 2-6
The 3-D Plot of the Calculated Intensity Distribution in an SMCWA, Using Experimental Parameters of Figure 2-5.

To ensure a required interconnect length, the channel separation in a SMCWA must be large enough to avoid significant channel cross-coupling. Therefore, in designing a SMCWA, it is necessary to find the minimum required channel separation, so that multiple channel crosstalk can be minimized and a desired SNR can be achieved for the desired interconnection length. Figure 2-7 is a plot of maximum channel length versus the SNR for several values of channel separation, and is based on Eq. (2-9) using the experimental parameters. The interconnect length of the SMCWA must be limited to about 0.1 cm in order to ensure a 32 dB SNR. To have channel length longer than 5 cm while maintaining an SNR above 32 dB, the minimum channel separation must be increased from 8 μm to 12 μm. Therefore, the channel packaging density of the SMCWA fabricated in our experiment could have been up to 700 channels/cm with channel lengths close to 5 cm and an SNR above 32 dB. The effect of waveguide propagation losses is not considered in this paper. Such losses will, however, change the system power budget, rather than the crosstalk effect considered herein.

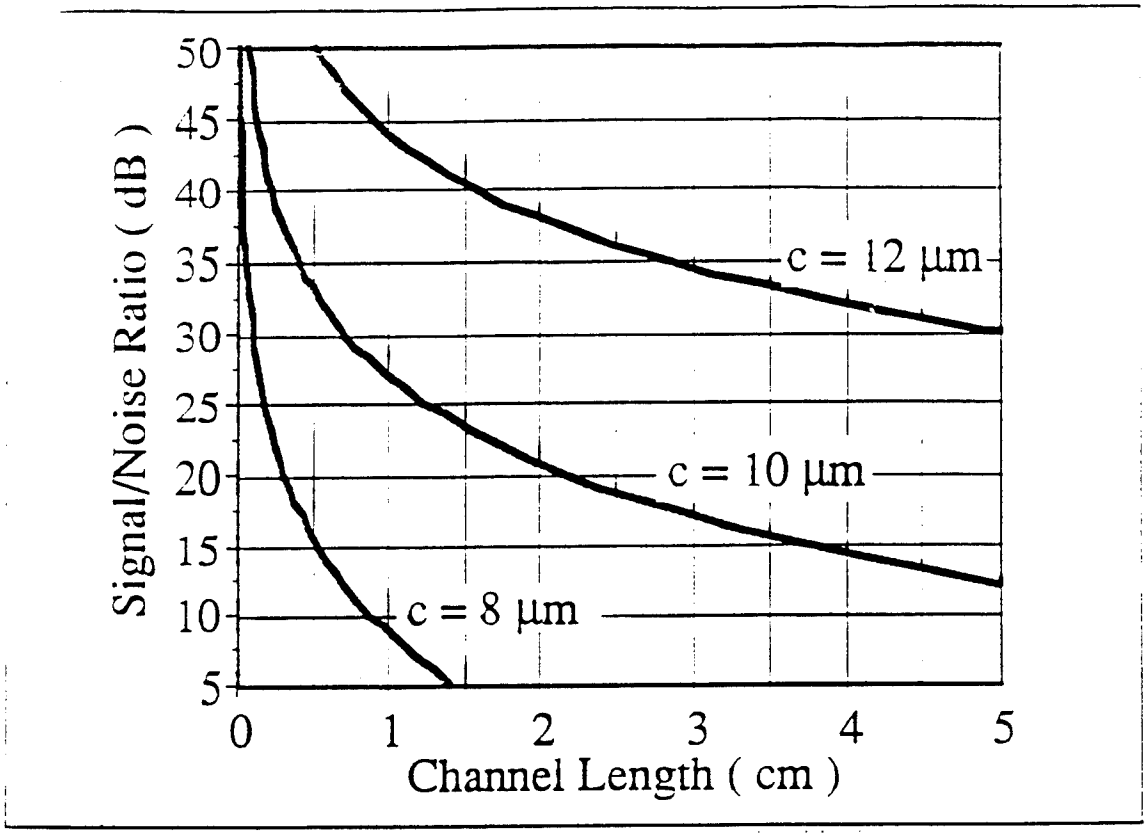

Figure 2-7
Signal/Noise Ratio Versus Maximum Channel Length with Channel Separation as a Parameter, Based on Equation (2-9). n_1 =1.5, n_2 =1.0, Δn = 0.004, a = 2 μm, c = 8 μm, 10 μm and 12 μm at λ = 1.3 μm were assumed.

The minimum channel separation (MCS) and maximum channel length (MCL) of a densely packed SMCWA have been studied using a multiple channel cross-coupling model together with experimental results. Because of the cross-coupling among densely packed channel waveguides, the optical interconnection distance (i.e., channel waveguide length) is not independent of packaging density. The spatial threshold for channel separation depends on the operating wavelength, channel dimensions, and the index difference between guiding layer and cladding layers to obtain a required interconnection distance for a typical polymer-based SMCWA, with n_1 = 1.5, n_2 = 1.0, and Δn ≈0.01 to 0.001. Experimental results are provided to verify the theory presented.

3.0 WAVEGUIDE DESIGN, OPTIMIZATION AND FABRICATION

The optical waveguide is an integral part of the proposed modulator/switch. Much attention has been paid in this project to the development a precise fabrication method for singlemode waveguide arrays and modulators. As a part of this effort, POC has developed a unique software package that

enables any user to design and optimize different types of waveguides, including raised strip, embedded strip, buried type, and ridge waveguides. POC's WaveDesign™ software is Microsoft Windows™ compatible, and provides a user-friendly interface with pull down menus.

3.1 WaveDesign™ Software Development

Waveguide design and optimization is an important part of any integrated optics development effort. Noting this important factor, POC was able to develop a unique software package that provides comprehensive computer aided design (CAD) in order to ease the complexity of single and multimode waveguide optimization. This software package enables a user to select a variety of waveguide geometries, as well as different material types for the final testing. This section describes the computer program written at POC for the purpose of identifying and analyzing the propagation modes of optical channel waveguides. The WaveDesign™ software runs on IBM PC-compatible machines (80386 or later) under Microsoft Windows™. It is written in Smalltalk, an object-oriented programming language; the development system used is from Digitalk. The modes are computed using a combination of the Marcatili method and the effective index method. Using this software, field profiles and mode dispersion data are obtained.

3.1.1 Installation

POC's WaveDesign™ software consists of one executable file, POCCWA.EXE, and nine dynamic link libraries (.DLL), for a total of ten files. To install the software, copy the files from the floppy disk to a single subdirectory of the machine's hard drive; for example, C:\POC\BIN. Once the files have been copied to the hard drive, the executable may be run from the Windows run command; however, it is convenient to create a desktop icon for it in the standard way.

3.1.2 Operation

When initially run, the WaveDesign™ program shows a single menu item, File, several tool icons on the toolbar, and a blank area. To analyze a channel waveguide, one creates a new *waveguide browser* in one of two ways: by selecting New from the File menu, or by pressing one of the tool icons. At present, three types of channel waveguides are supported: ridge waveguides; buried waveguides; and dielectric-strip loaded waveguides. These are listed by name under File/New, which is a walking menu, and represented pictorially by the tool icons.

When requesting the creation of a new browser, the user is prompted for information describing the waveguide geometry and material properties (refractive indices). In addition, the user is asked to specify a set of wavelengths (or normalized frequencies – see below) for which the mode structures are to be calculated. For convenience, and for illustrative purposes, these data have typical values, as defaults as shown in Figure 3-1.

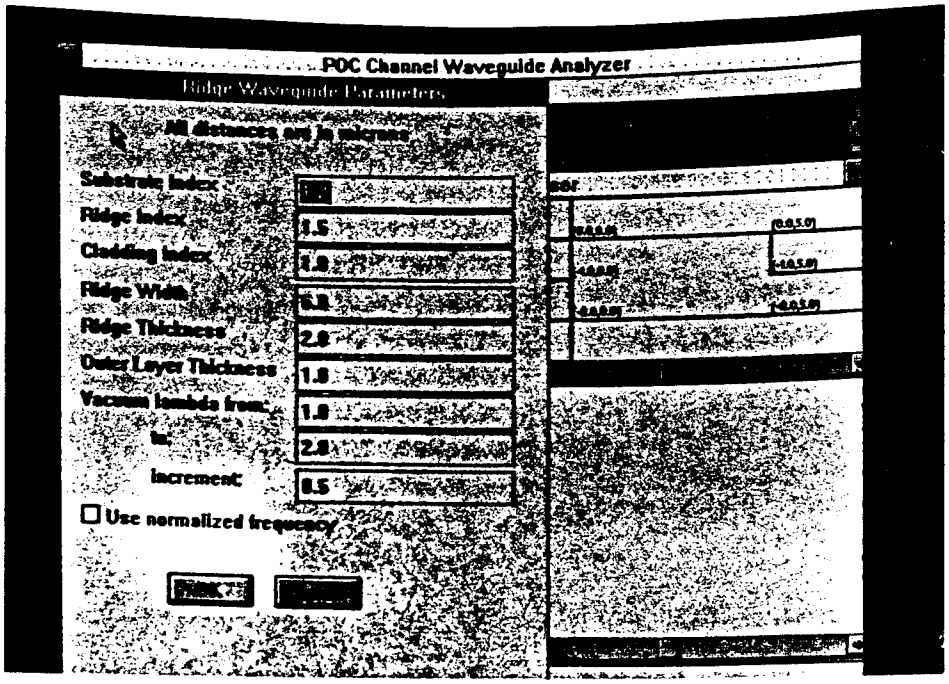

Figure 3-1
POC's Channel Waveguide Analyzer. To initiate the waveguide design, a list of parameters must be entered

The refractive indices may be entered either as a number (e.g. 1.33), in which case the constant value is used, or as a string (e.g. 'GaAs'), denoting a preconfigured material type. The latter case is preferable, because the values need not be looked up by the user, but more importantly, because then the material's dispersion is correctly taken into account when a range of wavelengths is specified. The material types recognized by WaveDesign™ are found in a text file 'material.def,' which is located in the working directory. For each recognized material type, a list of points is given, where the abscissa is the wavelength in microns and the ordinate is the corresponding refractive index. WaveDesign employs linear interpolation for wavelengths between the points given in the file. The material definition file is created automatically if not present; once in existence, it may be modified and extended by the user and will not be overwritten by WaveDesign™.

When the data in the dialog box are as desired, the user selects OK or hits the Enter key in order to initiate computation of the mode structure, or Cancel to abort. When the computation is complete, a waveguide browser appears. The browser is a tool for tabulating the propagating modes and visualizing their field profiles.

To use the waveguide browser, one must first select the wavelength at which the mode structure is desired. The wavelengths which were previously chosen in the data entry dialog box are now listed in the leftmost list box of the browser, below the polarization selection box (see Figure 3-2).

When one of the wavelengths is selected, the second list box shows the list of p indices for which stationary modes exist. (The index p is the mode index, or number of modes, in the vertical or x-direction.) The index p=0 is preselected. The third list box shows the list of q values (mode indices for the horizontal or y-direction) for which a mode exists for the selected p. By default, the vertically polarized modes are presented; either polarization may be selected at any time by pushing the appropriate polarization button at the upper left.

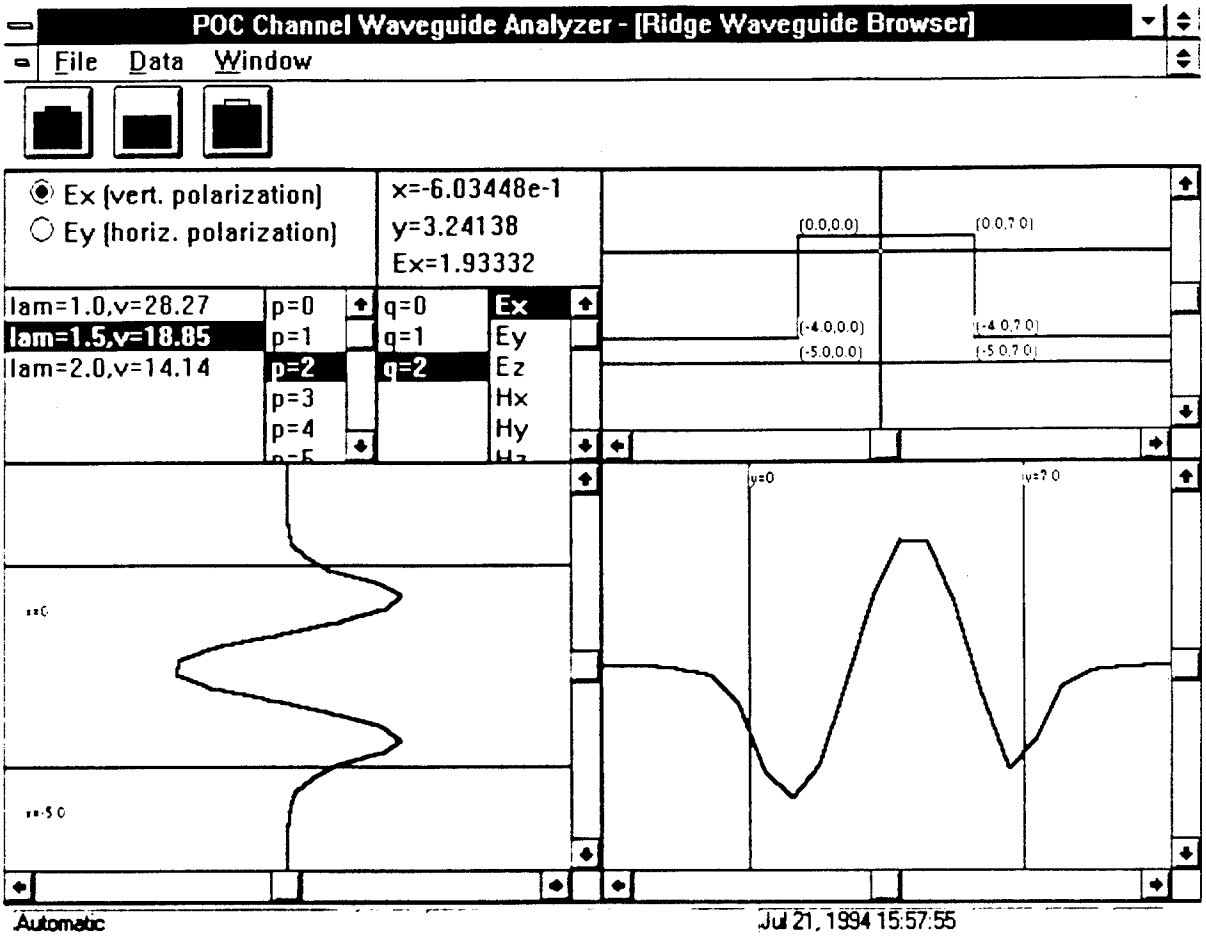

Figure 3-2
Screen Arrangement for the POC's Channel Waveguide Analyzer Drawing Optimization of Three Different Types of Waveguides

The total number of propagating modes for the selected wavelength and polarization is obtained by selecting each p value and summing the number of q values listed for each.

When a mode (p and q) is selected, the amplitude profile of any desired field component may be visualized. The E_x component is preselected; any component of the electric field E and the magnetic field H may be selected in the fourth list box. The profile is presented as two-

dimensional slices of the three-dimensional profile (for example, E_x as a function of x and y) in the vertical and horizontal directions, displayed in two large panes at bottom. The location of the slicing planes is shown in the small pane to the right of the list boxes, in which a line drawing of the waveguide structure is displayed along with a crosshair cursor. The cursor may be moved by clicking or dragging the left mouse button; the field profile plots attempt to keep up with the mouse motion. The current cursor position is shown at top center.

A file containing the field profile of the currently displayed mode and field component may be obtained using the Field Amplitudes menu item under the Data menu. The file is stored in a Microsoft Excel file format, and contains the field amplitude at each point in a two-dimensional grid of points covering the channel and the surroundings.

A file containing the mode dispersions may be obtained. The dispersion is the variation of effective propagation index n_{eff} with the vacuum wavelength λ. Here, these quantities are normalized according to the custom established in the literature [12]: the normalized frequency is given by $V = (2\pi d/\lambda)(n_1^2 - n_2^2)^{1/2}$, where d is the waveguide channel thickness, n_1 is the channel refractive index (guide index), and n_2 is the substrate index. The normalized propagation constant is given by

$$\frac{n_{eff}^2 - n_2^2 k^2}{(n_1^2 - n_2^2)k^2} \tag{3-1}$$

where $k = 2\pi/\lambda$ is the wavenumber. Thus, mode dispersion is the variation of normalized propagation constant with normalized frequency.

Mode dispersion data may be obtained by selecting Mode Dispersion from the Data menu. This brings up a filename selection dialog box. The dispersion data are stored in the selected filename in Microsoft Excel file format, which is read by standard Windows plotting packages.

Multiple waveguides may be analyzed simultaneously by creating multiple browsers. The browsers may be resized and placed next to each other or overlapping as desired. The standard Cascade and Tile operations for multiple windows are available in the Window menu.

3.1.3 Algorithm

Two approximate methods are commonly used in the investigation of channel waveguides of rectangular geometry: The effective index method [12] and the Marcatili method [12,13]. WaveDesign™ employs a combination of these two methods, which will be explained below.

3.1.3.1 Effective Index Method

Consider the geometry shown in Figure 3-3, in which a channel of refractive index n_1 is surrounded by materials of refractive index $n_2 \cdots n_5$. The effective index method calculation of the channel modes proceeds in two steps.

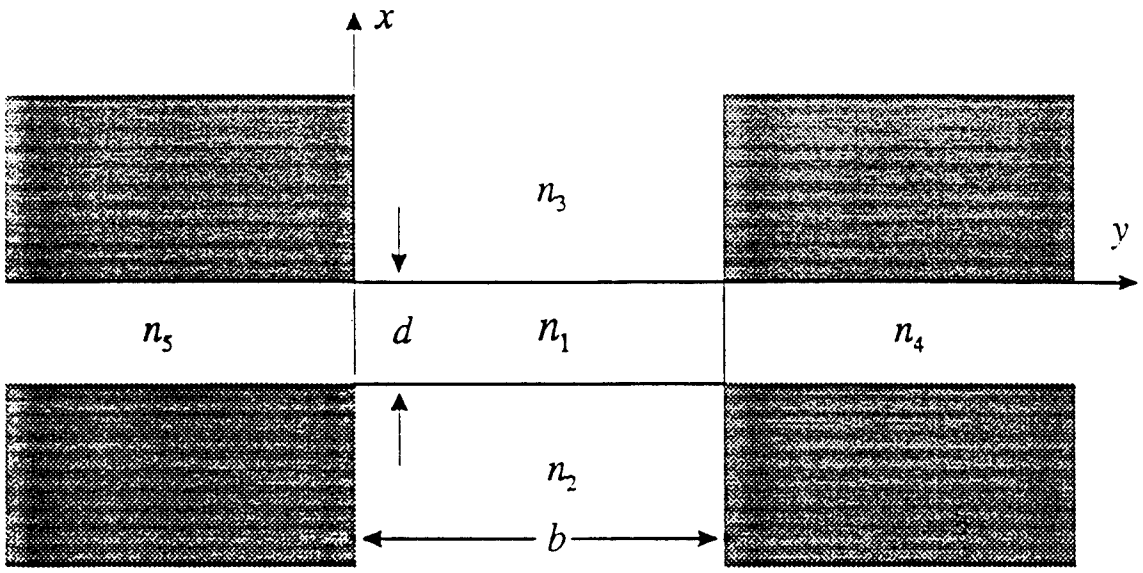

Figure 3-3
Rectangular-Geometry Channel Waveguide

The mode structure will be dominated by the smaller dimension d; to a first approximation, the modes resemble those of the one-dimensional planar waveguide obtained by letting $b \rightarrow \infty$ (Figure 3-3). The first step is to solve this one-dimensional problem, which can be done exactly [12]. This yields a set of effective indices $n_{eff,p}$ for propagating modes in the one-dimensional waveguide, where p is the mode index in the x-direction.

The second step of the effective index method is to make an approximation for each of the one-dimensional modes. Then, the channel waveguide may be approximated by the planar waveguide shown in Figure 3-4 (b). For each value of p (each propagating mode in the one-dimensional waveguide of Figure 3-4 (a)), a set of y-direction modes indexed by q is obtained; for a given p, this set may be empty.

The result of the effective index method, then, is a set of effective indices $n_{eff,pq}$ of mode propagation. Note that modes which are TE (transverse-electric) in the first step are TM (transverse-magnetic) in the second step, and vice versa; thus, the two polarizations of the channel waveguide modes are taken into account.

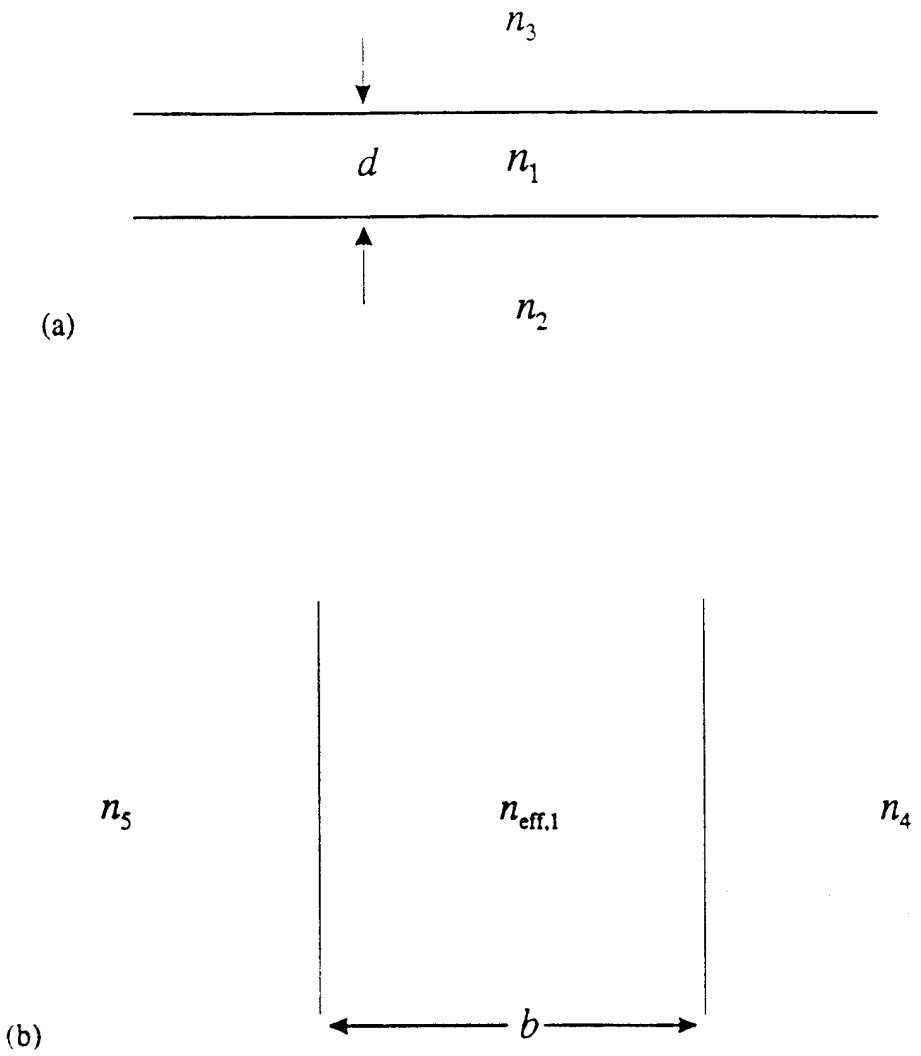

Figure 3-4
(a) One-Dimensional Waveguide for First Step of Effective Index Method
(b) Waveguide for Second Step, Using Effective Index From the First Step

3.1.3.2 Marcatili Method

In the Marcatili method, the approach is to assume that the propagating modes of the channel waveguide have wavefunctions (the fields $\bar{E}_{pq}(x,y)$ and $\bar{H}_{pq}(x,y)$), which are products of wavefunctions that are separately functions of x and y; i.e., they separately satisfy the boundary conditions at the top and bottom edges of the channel and at the left and right edges:

$$\bar{E}_{pq}(x,y) \equiv \bar{E}_p(x)\bar{E}_q(y) \tag{3-2}$$

and similarly for $\bar{H}_{pq}(x,y)$. Note that this approximation implies that the boundary conditions in the shaded regions of Figure 3-3 will not be exactly satisfied. Thus, the Marcatili method is valid only for modes which are far from cutoff, where the fraction of the total energy in those regions is low.

The Marcatili method provides analytical formulas for the fields $\bar{E}_{pq}(x,y)$ and $\bar{H}_{pq}(x,y)$, for both E_x and E_y polarizations, in each of the five numbered regions of Figure 6-3. These expressions are quite lengthy; we give here expressions for the field components of the E^x_{pq} mode in the channel itself (region 1). A more complete tabulation is found in Ref. [12]. This set is still not complete; however, the full set of functions are available on request.

$$E_x = \frac{iA}{\kappa_x \beta}\left(n_1^2 k^2 - \kappa_x^2\right)\sin\kappa_x(x+\xi)\cos\kappa_y(y+\eta)e^{i(\omega t-\beta z)} \tag{3-3a}$$

$$E_y = \frac{-iA\kappa_x}{\beta}\left(n_1^2 k^2 - \kappa_x^2\right)\cos\kappa_x(x+\xi)\sin\kappa_y(y+\eta)e^{i(\omega t-\beta z)} \tag{3-3b}$$

$$E_z = A\cos\kappa_x(x+\xi)\cos\kappa_y(y+\eta)e^{i(\omega t-\beta z)} \tag{3-3c}$$

$$H_x = 0 \tag{3-3d}$$

$$H_y = iA\sqrt{\frac{\varepsilon_0}{\mu_0}}n_1^2\frac{k}{\kappa_x}\sin\kappa_x(x+\xi)\cos\kappa_y(y+\eta)e^{i(\omega t-\beta z)} \tag{3-3e}$$

$$H_z = -A\sqrt{\frac{\varepsilon_0}{\mu_0}}n_1^2\frac{\kappa_y}{\kappa_x}\frac{k}{\beta}\sin\kappa_x(x+\xi)\sin\kappa_y(y+\eta)e^{i(\omega t-\beta z)} \tag{3-3f}$$

In the above, A is an arbitrary multiplicative constant; $k^2 = \omega^2\varepsilon_0\mu_0$; and $\beta^2 = n_1^2k^2 - \kappa_x^2 - \kappa_y^2$.

The values of the transverse wavenumbers κ_x and κ_y are obtained in the Marcatili method by solving the eigenvalue equation

$$\tan\kappa_x d = n_1^2\kappa_x\frac{n_3^2\gamma_2 + n_2^2\gamma_3}{n_3^2n_2^2\kappa_x^2 - n_1^4\gamma_2\gamma_3} \tag{3-4}$$

where $\gamma_i = \left[\left(n_1^2 - n_i^2\right)k^2 - \kappa_x^2\right]^{1/2}$, with a similar equation for κ_y.

In the above, the parameters ξ and η are given by

$$\tan\kappa_x\xi = -\frac{n_3^2\kappa_x}{n_1^2\gamma_3} \quad \text{and} \quad \tan\kappa_x\eta = -\frac{\gamma_5}{\kappa_y} \tag{3-5}$$

3.1.3.3 Hybrid Method Used in WaveDesign™

As mentioned, WaveDesign™ employs a combination of the effective index and Marcatili methods. It has been found [12] that the propagation constants β_{pq} and $n_{eff,pq}$ obtained by the effective index method are more accurate than those of Marcatili. However, the Marcatili expressions for the fields are the more accurate. For this reason, we find the values of κ_x and κ_y using the effective index method and use these values in the Marcatili expressions for the fields.

3.1.3.4 Structure of WaveDesign™ Source Code

As mentioned above, WaveDesign™ is written in Digitalk Smalltalk. This allowed objects (data types with specific behaviors) to be constructed for each physical element of the problem under study. The collection of object specifications, along with a graphical user interface, constitutes WaveDesign™.

The types of objects defined in WaveDesign™ are shown in Table 3-1. The object description given there is abbreviated, in that it does not describe the methods (functions) available to each class of object.

Table 3-1. Object types used in WaveDesign™

Object Class	Subclass of	Description
ScienceObject	Object	General data type used for scientific simulation
ChannelWaveguide	ScienceObject	Two-dimensional rectangular channel waveguide
BuriedWaveguide	ChannelWaveguide	Buried-channel waveguide
DielectricStripLoadedWaveguide	ChannelWaveguide	Dielectric-strip-loaded waveguide
RidgeWaveguide	ChannelWaveguide	Ridge waveguide
Mode	ScienceObject	Mode of channel waveguide
ModeList	ScienceObject	A container for two two-dimensional arrays of Modes, one for the E_x polarization and one for the E_y
PlanarWaveguide	ScienceObject	One-dimensional infinite slab waveguide
MDIWaveguideView	MDIViewManager	Graphics manager for entire program
WaveguideBrowser	ViewManager	The waveguide browser
WaveguideDialog	WindowDialog	Dialog box for entering the geometry and material properties for a channel waveguide

The program's flow of control is as follows. The main program is initiated by the creation of an MDIWaveguideView, which represents the main window of the program. This main window contains the menu bar, the tool bar, and an area for the waveguide browsers. Pushing of a tool icon or selection of File/New... results in the creation of an appropriate WaveguideDialog for entry of waveguide configuration data. Upon closure, a new WaveguideBrowser is created, and a corresponding instance of the appropriate subclass of ChannelWaveguide (BuriedWaveguide, DielectricStripLoadedWaveguide, or RidgeWaveguide) is initialized with the defining data selected in the WaveguideDialog.

As part of the creation of the WaveguideBrowser, the waveguide mode structure is calculated. This is accomplished by sending it the message *modes: lambda*, where *lambda* is a wavelength value for each wavelength in the chosen range of wavelength or normalized frequency. In order to avoid repetition of the mode calculation if the user is jumping among wavelengths, previously calculated mode structures are maintained in a dictionary, whose keys are wavelengths and whose values are ModeLists.

The real work of mode calculation is distributed. For the implementation of the effective index method, the modes of one-dimensional slab waveguides are needed; object class PlanarWaveguide handles this job. The most difficult problem here is the solution of the eigenvalue equation for the transverse wavenumber. The result of this calculation is a list of planar waveguide propagation constants. This is used by WaveDesign™ in the method *modeConstants:type*, in which PlanarWaveguides are created for both steps of the effective index method.

The mode constants are needed in the creation of channel waveguide mode lists. A mode is a holder for functions representing the field components; these functions are symbolically defined by WaveDesign™, and to be evaluated, they require numerical values to be substituted into their definitions. This is done by WaveDesign *modes:type*, which first calls *modeConstants:type:* to obtain the mode propagation constants.

The entire code listing is given in Appendix A. Selected method listings are given in Figures 3-5, 3-6, and 3-7.

```
modeConstants: lambda type: type
    "Answer an array of mx arrays, where mX is the number of modes (type 1:
Ex; 2: Ey)
    in the x-direction (p=0,1,2,...,mx). Each of the mx arrays contains the
my
    mode constant arrays of the allowed modes in the y-direction for the given
p
    (q=0,1,2,...,my(p)). If my(p)=0, the pth array is nil.

    A mode constant array has the form (Kx, Ky, Neff)."

        | kx nEff props modeConstants centerPropagationConstants k
effectiveIndices array wg mX left |
    k := 2 * Pi / lambda.

        (centerPropagationConstants := self centerPlanarWaveguide
propagationConstants: lambda type: 3 - type)
        isNil ifTrue: [^nil].

    mX := centerPropagationConstants size.

    (left := self leftEffectiveIndex: lambda type: 3 - type) isNil ifTrue:
[^nil].

    wg := PlanarWaveguide new
        d: guideWidth;
        ns: left;
        nc: left.

    modeConstants := Array new: mX.

    1 to: mX do: [ : p |
        kx := (centerPropagationConstants at: p) at: 1.
        nEff := (centerPropagationConstants at: p) at: 2.
        wg nf: nEff.
        modeConstants at: p put: (array := wg propagationConstants: lambda
type: type).
        array isNil ifFalse: [
            1 to: array size do: [ : q |
                props := array at: q.
                array at: q put: (Array new: 3).
                (array at: q) at: 1 put: kx.
                (array at: q) at: 2 put: (props at: 1).
                (array at: q) at: 3 put: (props at: 2).
            ]
        ]
    ].

    ^modeConstants
```

Figure 3-5
ChannelWaveguide Method *ModeConstants:Type*, in Which the Propagation Constants for the Channel Waveguide Modes are Determined.

```
modes: lambda type: type
    "Answer an array of mx arrays, where mx is the number of modes (type 1:
Ex; 2: Ey)
    in the x-direction (p=0,1,2,...,mx). Each of the mx arrays contains the
my
   allowed Modes in the y-direction for the given p
    (q=0,1,2,...,my(p)). If my(p)=0, the pth array is nil.

    To recover the mode Ex(p,q) for a given waveguide,
        mode := ((waveguide modes: lambda type: 1) at: p) at: q
     is appropriate. Check for nils first because q-arrays are of varying
size."

    | top bottom left right parser
    mode modes qArray kx ky nEff beta props
    funcs g2 g3 g4 g5 xi eta k |

    parser := FunctionParser new
        assign: 'e0' value: Epsilon0;
        assign: 'mu0' value: Mu0;
        assign: 'd' value: guideThickness;
        assign: 'b' value: guideWidth;
        assign: 'k' value: (k := 2 * Pi / lambda);
        assign: 'n1' value: guideIndex;
        assign: 'n2' value: (bottom := self bottomIndex);
        assign: 'n3' value: (top := self topIndex);
        assign: 'n5' value: (left := self leftEffectiveIndex: lambda type: (3
- type));
        assign: 'n4' value: (right := left).

    (modes := self modeConstants: lambda type: type) isNil ifTrue: [^nil].

    1 to: modes size do: [ : p |
        (qArray := modes at: p) isNil ifFalse: [
            1 to: qArray size do: [ : q |
                props := qArray at: q.
                parser
                    assign: 'kx' value: (kx := props at: 1);
                    assign: 'ky' value: (ky := props at: 2);
                    assign: 'beta' value: (beta := ( (k * guideIndex) squared
- (kx squared) - (ky squared) ) sqrt);
                    assign: 'nEff' value: (nEff := props at: 3);
                     assign: 'g2' value: (g2 := (ky squared + beta squared -
(bottom * k) squared) sqrt);
                     assign: 'g3' value: (g3 := (ky squared + beta squared -
(top * k) squared) sqrt);
                     assign: 'g4' value: (g4 := (kx squared + beta squared -
(right * k) squared) sqrt);
                     assign: 'g5' value: (g5 := (kx squared + beta squared -
(left * k) squared) sqrt);
```

```
                    assign: 'xi' value: (
                        (type = 1)
                            ifTrue: [ ((top / guideIndex) squared * kx / g3)
negated arcTan / kx]
                            ifFalse: [(g3 / kx) arcTan / kx]
                    );
                    assign: 'eta' value: (
                        (type = 1)
                            ifTrue: [(g5 / ky) negated arcTan / ky]
                            ifFalse: [((left / guideIndex) squared * ky / g5)
arcTan / ky]
                    ).
                funcs := Array new: 6.
                1 to: 6 do: [ : i |
                    funcs at: i put: (Function new expression: ((self class
functions at: type) at: i) deepCopy).
                    self class newParserArguments: parser func: (funcs at: i).
                        (funcs at: i) expression replaceIdentifiers: parser
symbolTable.
                ].
                qArray at: q put: (
                    mode := Mode new owner: self;
                        kx: kx;
                        ky: ky;
                        nEff: nEff;
                        functions: funcs
                ).
            ]
        ]
    ].
    ^modes
```

Figure 3-6
Channel Waveguide Method *Modes:Type*, in Which the Functions Describing the Field Components are Copied and Initialized

```
functions
      "Answer an array containing two arrays, each containing six mode
expressions
    (Ex,Ey,Ez,Hx,Hy,Hz).
    The first of the two arrays is for the Ex modes, and the second, for the
Ey modes.
    These expressions contain identifiers such as kx, g2, etc. In order to
    be used, they must be deepCopied and sent the message replaceIdentifiers:
symbolTable
      where symbolTable is a Dictionary containing the values for each
identifier.

    The mode expressions give the Marcatili fields for a rectangular channel
waveguide.
    For the source of these expressions, see Marcuse, 'Theory of Dielectric
    Optical Waveguides,' pp. 51--54."

    | parser exFunctions eyFunctions |

    Functions isNil ifTrue:  [
        CursorManager execute change.
        Functions := Array new: 2.
        parser := FunctionParser new.

        exFunctions := Array new: 6.
        Functions at: 1 put: exFunctions.
        exFunctions at: 1 put:  "Ex"
            (parser parseWithoutReplacing: '
                @ifelse( x < -d,
                          (g2^2 + (n2*k)^2 ) / (g2*beta) * @cos(kx*(xi-d)) *
@cos(ky*(y+eta)) * @exp(g2*(x+d)),
                @ifelse( x > 0,
                            -(g3^2 + (n3*k)^2) / (g3*beta) * @cos(kx*xi) *
@cos(ky*(y+eta)) * @exp(-g3*x),
                @ifelse( y > b,
                              (n1/n4)^2 * ((n4*k)^2 - kx^2) / (kx*beta) *
@cos(ky*(b+eta)) * @sin(kx*(x+xi)) * @exp(-g4*(y-b)),
                @ifelse( y < 0,
                     (n1/n5)^2 * ((n5*k)^2 - kx^2) / (kx*beta) * @cos( ky*eta)
* @sin(kx*(x+xi)) * @exp(g5*y),
                         ((n1*k)^2 - kx^2) / (kx*beta) * @sin(kx*(x+xi)) *
@cos(ky*(y+eta))
                ))))'
            ).

        exFunctions at: 2 put:  "Ey"
            0.
```

```
        exFunctions at: 3 put:  "Ez"
            (parser parseWithoutReplacing: '
                @ifelse( x < -d,
                    @cos(kx*(xi-d)) * @cos(ky*(y+eta)) * @exp(g2*(x+d)),
                @ifelse( x > 0,
                    @cos(kx*xi) * @cos(ky*(y+eta)) * @exp(-g3*x),
                @ifelse( y > b,
                      (n1/n4)^2 * @cos(ky*(b+eta)) * @cos(kx*(x+xi)) * @exp(-
g4*(y-b)),
                @ifelse( y < 0,
                    (n1/n5)^2 * @cos( ky*eta) * @cos(kx*(x+xi)) * @exp(g5*y),
                @cos(kx*(x+xi)) * @cos(ky*(y+eta))
                ))))'
            ).

               CursorManager normal change
    ].
    ^Functions
```

Figure 3-7
ChannelWaveguide Cass Method *Functions*, in Which the Functions Describing the Field Components are Created. The method listing is abbreviated to show only the electric fields in the E_x polarization. Note the syntax for defining functions with different expressions for different spatial regions.

4.0 DESIGN, FABRICATION AND PACKAGING OF THE OPTICAL CROSSBAR SWITCH

4.1 The Working Principle of the Optical Switch

A discussion of the working principle of the modulator follows. A very large index change induced by current has been reported on Si [16,17], GaAs-GaAlAs [18], and InGaAsP-InP [19-21]. Since the current-induced index change is much stronger than the linear electro-optic effect, we can make an active device by injecting a time-dependent carrier concentration. The current is first induced by shining a strong condensed light with a photon energy larger than the band gap of the guiding layer material on the window area, as shown in Figure 4-1. In this way, a very large current density is induced. When the optical signal carrier to be modulated is coupled to the ridge waveguide, the induced current will interact with the guided wave.

The induced index change created by electron-hole pair generation can be written as

$$\Delta n = \frac{-2\pi N_e e^2}{m_e^* \omega^2 n_o} + \frac{-2\pi N_p e^2}{m_p^* \omega^2 n_o} \qquad (4\text{-}1)$$

where N_e and N_p represent the concentration of electrons and holes, respectively. By using the Kramers-Keonig relations, the absorption associated with free electrons and free holes is:

$$\Delta\alpha = \left(e^3\lambda^2 / 4\pi^2 C^3 \varepsilon_o n_o\right) \left[N_e / m_o^{*2} \mu_e + N_h / m_p^{*2} \mu_p\right] \qquad (4\text{-}2)$$

where e is the electron charge, ε_o is the permittivity of free space, μ_e is the electron mobility, and μ_p is the hole mobility. With an interaction length of 5 μm, the throughput intensity modulation is caused mainly by refractive index modulation (Eq. (4-1)), rather than absorption (Eq. (4-2)). It was proven in this program that the change of index of refraction due to the injected free carriers can be two orders of magnitude higher than that generated by the linear electrooptic (EO) effect. A device interaction length that is compatible with a multi-quantum well structure is achievable using this proposed concept.

Another important conclusion from Eq. (4-1) is that, in contrast to the linear electro-optic effect (which depends upon the vector electric field), the induced index change is a scalar function. If the effective masses of electrons and holes in the two different transverse directions are the same, then the induced change of the guiding layer index is the same for both TE and TM guided waves. This eases the requirement needed for the direction of waveguide propagation.

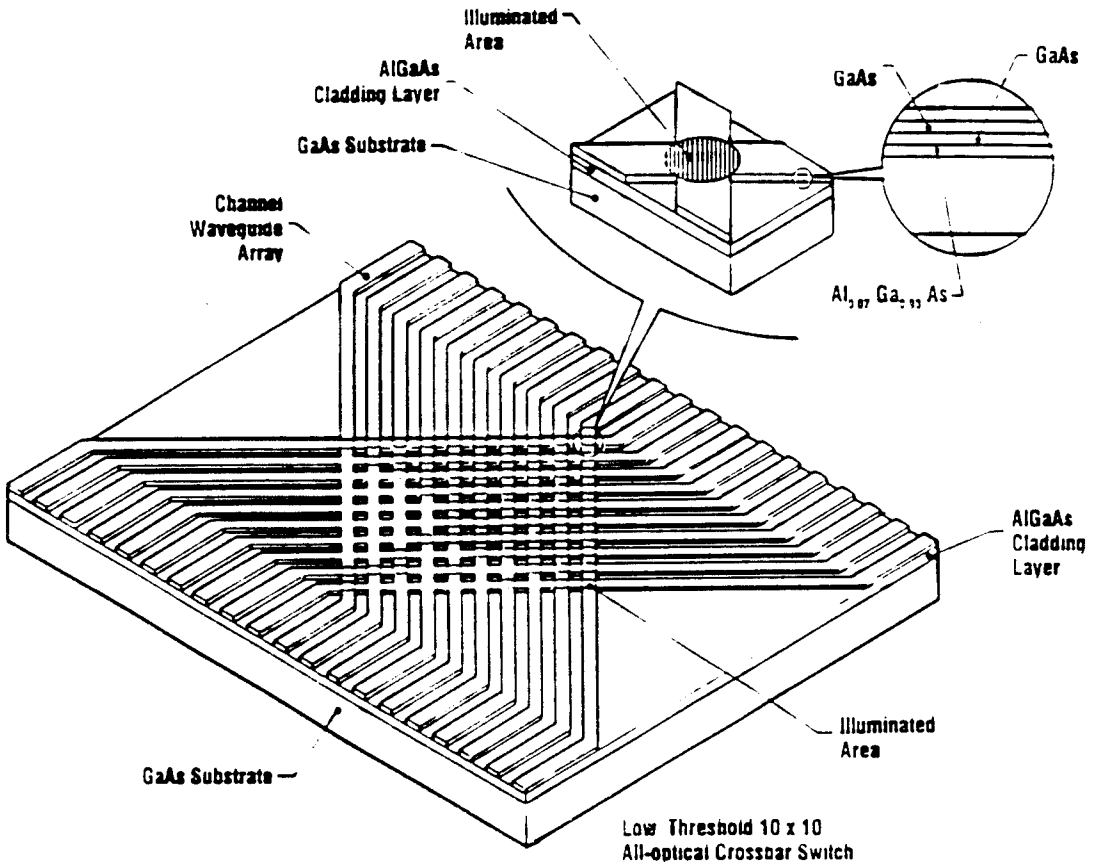

Figure 4-1
Low Threshold 10x10 All-Optical Crossbar Switch Designed in this Phase II Program

4.2 Channel Waveguide Design

From the experimental point of view, the key point of optimization of a singlemode channel waveguide at a given wavelength is the accuracy involved in determining the ΔN value at the wavelength of interest. In order to achieve the required accuracy, it is necessary to first theoretically determine the proper waveguide parameters, such as waveguide width and depth. The challenge here is to precisely determine the effective index of the guided mode at the desired optical wavelengths under various waveguide dimensions and cladding layer indices. Marcatili's method [22] is used to determine the upper boundary of the waveguide cut-off dimensions at 1.3 μm and 1.5 μm with Al concentrations equal to 5% and 7%. The results are displayed in Figures 4-2 and 4-3.

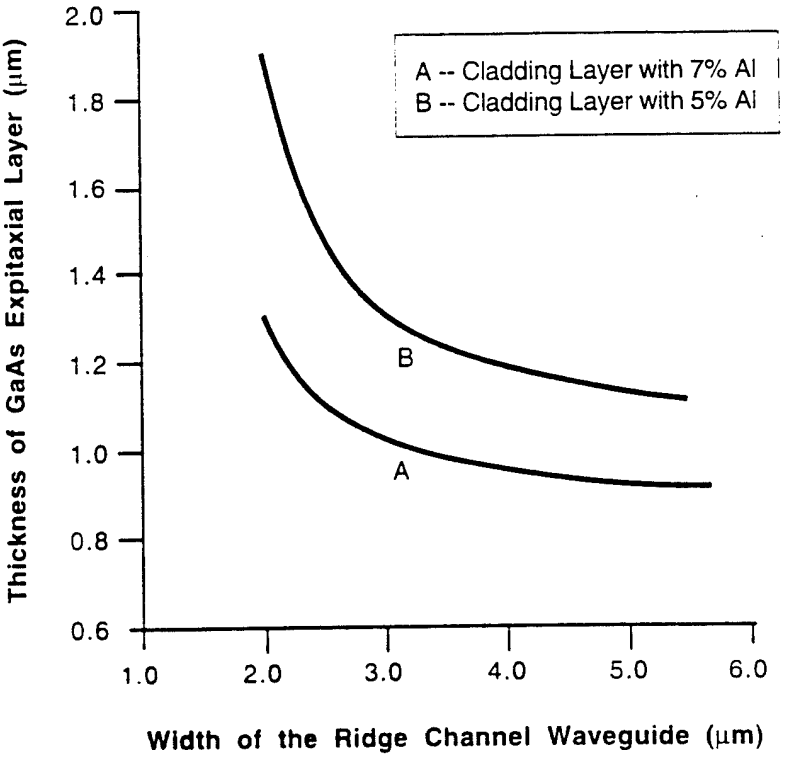

Figure 4-2
The Calculated Results of Cutoff Dimension on GaAs-GaAlAs Heterostructure Ridge Channel Waveguide with Al = 5% and 7% at 1.3 μm Wavelength

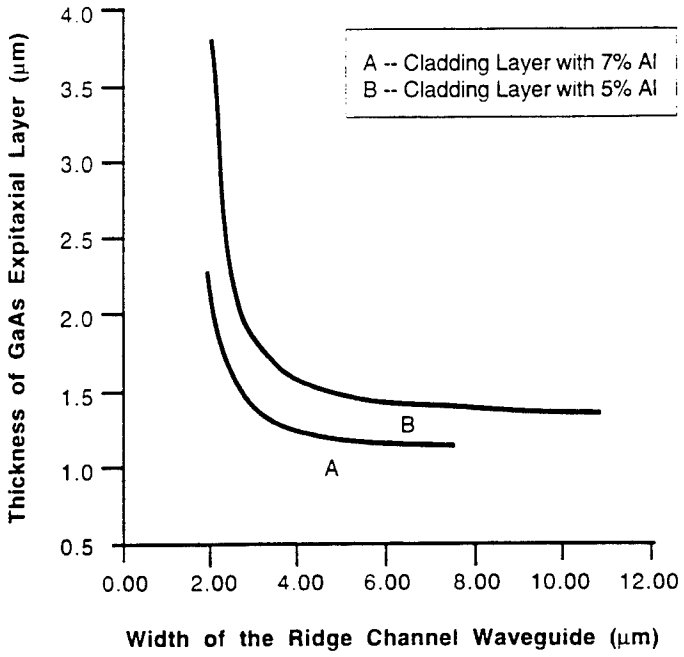

Figure 4-3
The Calculated Results of Cutoff Dimension on GaAs-GaAlAs Heterostructure Ridge Channel Waveguide with Al = 5% and 7% at 1.55 μm Wavelength

4.3 Material Design

The optical switch is grown on the GaAs substrate using the most advanced Metal Organic Chemical Vapor Deposition (MOCVD) technique. The material structures are shown in Table 4-1. First, a cladding layer ($Al_{0.07}Ga_{0.93}$) with a thickness of 1.5 μm is grown on the n^+ GaAs buffer layer. Then, a 4 μm undoped GaAs layer is grown as the guiding layer, which has a background doping under 10^{14} cm^{-3}. Then, the p^+ type base layer is grown, which is heavily doped to 10^{19} cm^{-3}. Above the base layer, an n type $Al_{0.25}Ga_{0.75}$ layer (to be used as the emitter) is grown with a doping density of 5×10^{17} cm^{-3} and a thickness of 2000Å . Finally, the n^+ GaAs capping layer is grown on the top. The material structures are verified by the polaron doping profiler. The measured thicknesses and doping concentrations are shown in Figure 4-4 . The emitter and base doping densities are close to the specified values.

Table 4-1. Epilayer Structure of the Multilayer Optical Switch

Ohmic Contact	2000 A	N^+ GaAs	1×10^{18} cm^{-3}
Emitter	2000 A	N^+ $A\ell_{0.25}Ga_{0.75}As$	5×10^{18} cm^{-3}
Photosensitive Base	1500 A	p GaAs	1×10^{18} cm^{-3}
Guiding Layer	40000 A	i GaAs	1×10^{14} cm^{-3}
Cladding Layer	15000 A	i $A\ell_{0.07}Ga_{0.95}As$	1×10^{14} cm^{-3}
Collector and Substrate	10000 A	n^+ GaAs	1×10^{18} cm^{-3}

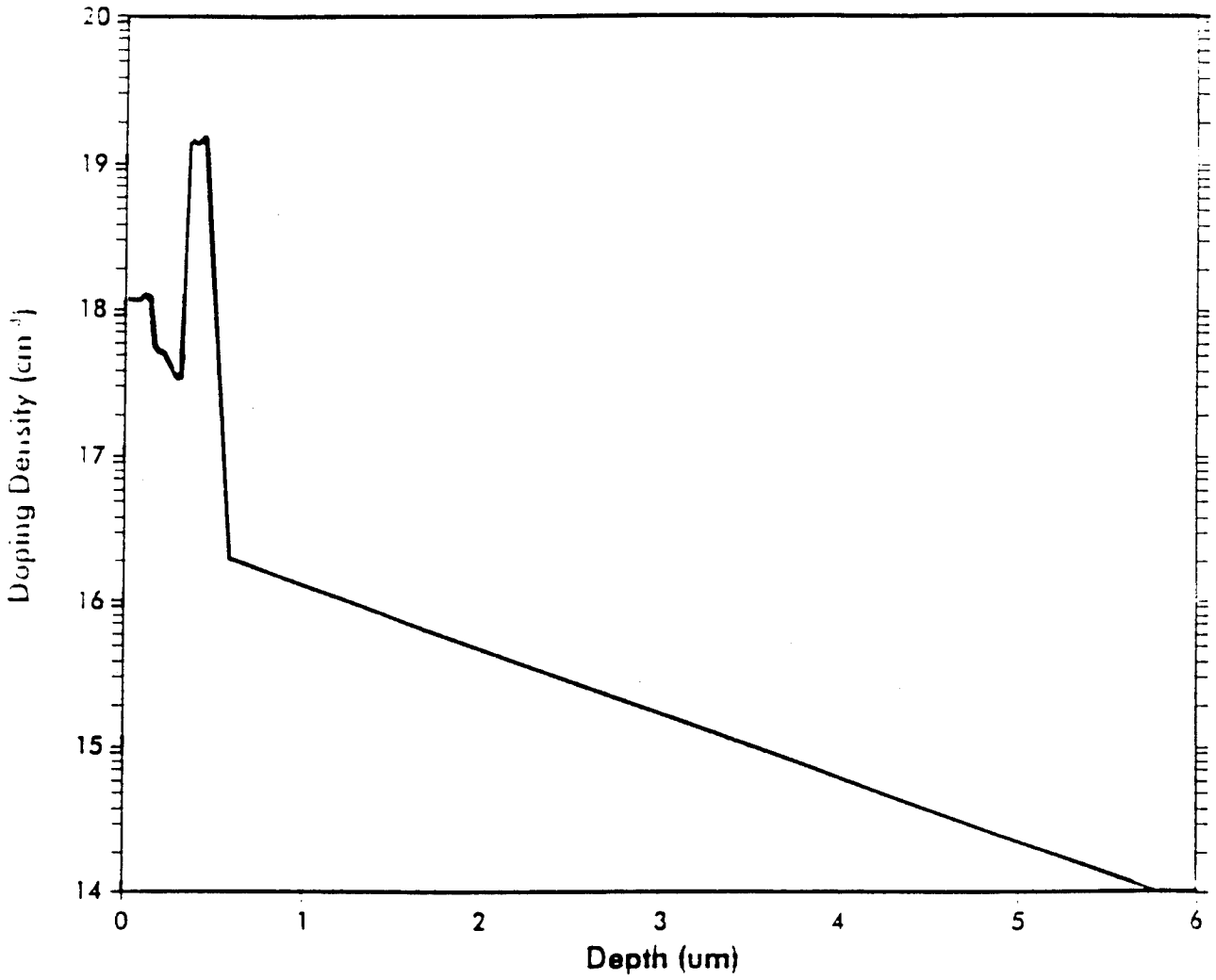

Figure 4-4
Carrier Doping Density Inside the Optical Switch Structure

4.4 Device Packaging

In the area of packaging, POC has developed a new assembly architecture for the alignment of, and the soldering between, singlemode fiber arrays and optical waveguide arrays, as illustrated in Figure 4-5. The assembly architecture has two key processes for optical coupling between the singlemode fiber arrays and the optical waveguide arrays; namely, alignment and fixing. Each process requires sub-μm precision, and typically has the following problems. First, the alignment between the arrays is very complicated, because their positions have six degrees of freedom, particularly, rotational degrees of freedom, which makes alignment more difficult. Soldering, which is typically used for fixing, can cause misalignments due to thermal shrinkage of the assembly equipment and solder volume. In order to solve these problems, an image position detection method is used to eliminate degrees of freedom for alignment. This allows the assembly

throughput to be much better than that of conventional assembly architectures. Also, the use of a thermal shrinkage compensation method achieves high-precision soldering by canceling misalignments caused by the thermal shrinkage of assembly equipment and solder volume.

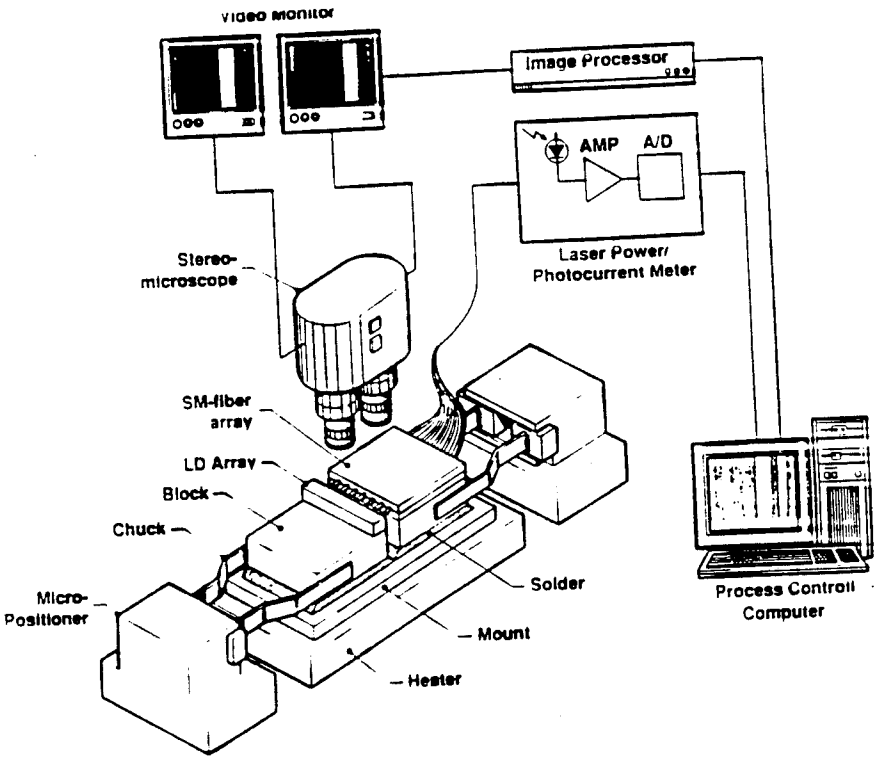

Figure 4-5
Illustration of Fiber/Waveguide Array Coupling System, for Coupling Between Fiber Ribbon (from Both Sides) and Integrated Optical Circuit

4.5 Singlemode Fiber Array

A schematic view of the singlemode fiber array is shown in Figure 4-6. The singlemode fiber array is sandwiched and soldered between two V-grooved silicon substrates.

The singlemode fiber has a 10 μm diameter core and a 125 μm diameter cladding. The V-grooves are formed on a silicon substrate through anisotropic etching using a KOH solution. They are designed to have 250 μm intervals and 160 μm depths. With careful silicon crystal orientation and control of the etching environment, the fiber arrangement can achieve ±0.5 μm precision.

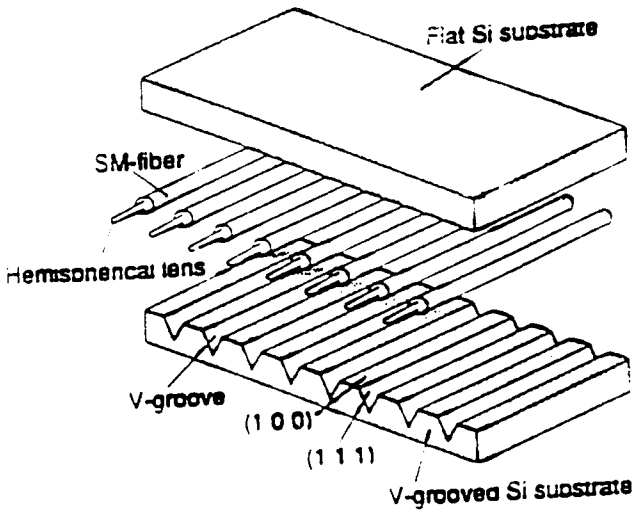

Figure 4-6
Schematic View of the SM-Fiber Array

Hemispherical lenses are formed at the fiber-ends in order to improve the optical coupling efficiency between the singlemode fiber array and the optical waveguide arrays. The lens formation process is shown in Figure 4-7. The fiber-ends are etched simultaneously using an HF solution, and then melted using an electric discharger. In pre-assembly, the singlemode fiber array is soldered onto the metal block.

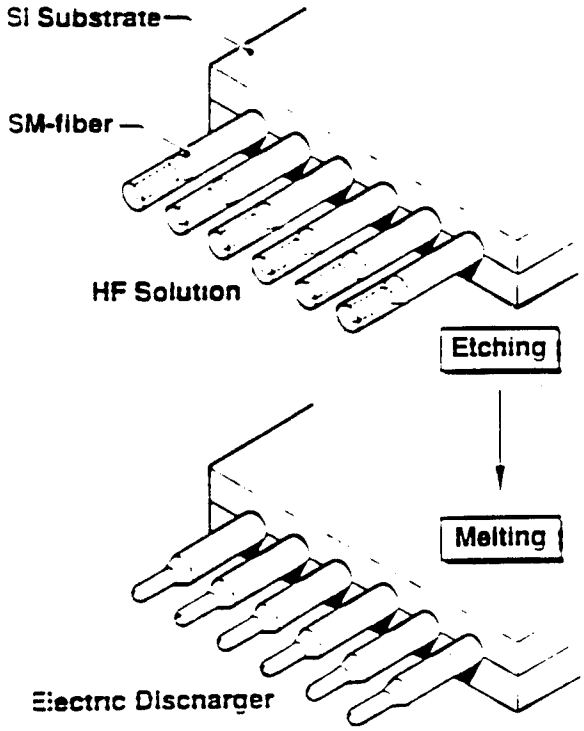

Figure 4-7
Hemispherical Lens Formation Process

4.6 Optical Coupling

Providing optical coupling with a maximum excess loss of 2 dB between the singlemode fiber array and the channel waveguide array requires a ± 1.5 μm precision. This precision must be achieved throughout the entire process: fiber arrangement, channel waveguide bending, alignment, and soldering. Each process, except for alignment, requires ± 0.5 μm precision. The coupling efficiency is remarkably changed by lateral misalignment of the X and Y axes, which are, respectively, parallel and vertical to the channel waveguide array. The efficiency change for the Z-axis is 10 times less remarkable than for the other axes.

4.7 Alignment

The alignment between the singlemode fiber array and the channel waveguide array is usually performed for six degrees of freedom: X, Y, Z (the linear axes), and θx, θy and θz (the rotational axes). Unfortunately, the alignment of the rotational axes interferes with the other axes, making the entire alignment procedure very time consuming. However, in POC's new architecture, the alignment for the Z, θ_X, and θ_Y axes is simplified, because a larger tolerance is allowed for these three axes.

In presetting before alignment, the single-mode fiber array block and the channel waveguide array are held by chucks, and the mount is set on a heater, as shown in Figure 4-8. The blocks can be independently moved for alignment. The blocks and chucks are precisely manufactured in order to eliminate the alignment for the θ_Y axis.

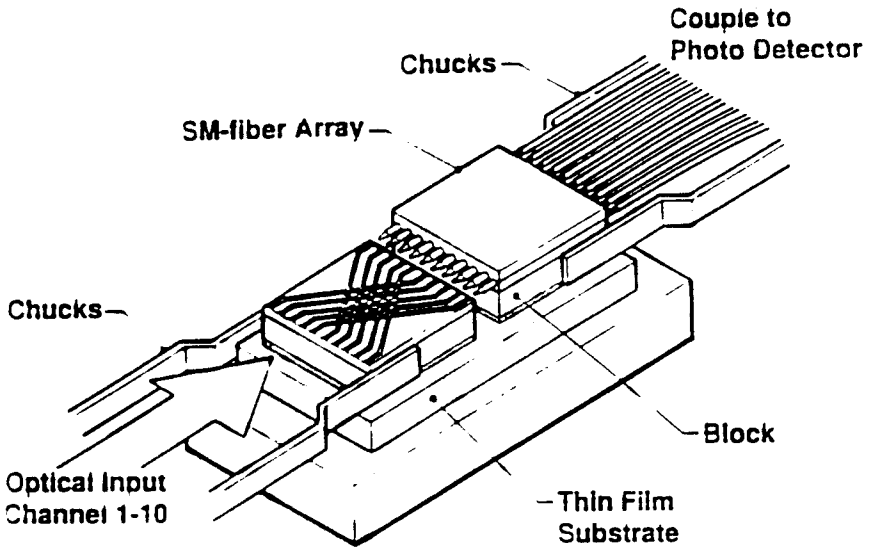

Figure 4-8
Soldering Process with the Thermal Shrinkage Compensation Method

The alignment process developed during this program is shown in Figure 4-9. In the process, rough alignment is performed prior to precise alignment in order to improve alignment throughout. The rough alignment achieves a ± 3 μm precision, which is sufficient for the Z and θy axes. The precision alignment uses the conventional active alignment method. By scanning the single-mode fiber array on the XY plane, the laser power meter measures the coupled laser power of the first and the last fibers. A 10 x 10 μm^2 area with a 0.5 μm interval is scanned. Misalignment for the X, Y and θz axes is corrected for using the (X,Y) position of the maximum laser power and the distance between the first and last channels. Thus, the array positions are correctly aligned without misalignments.

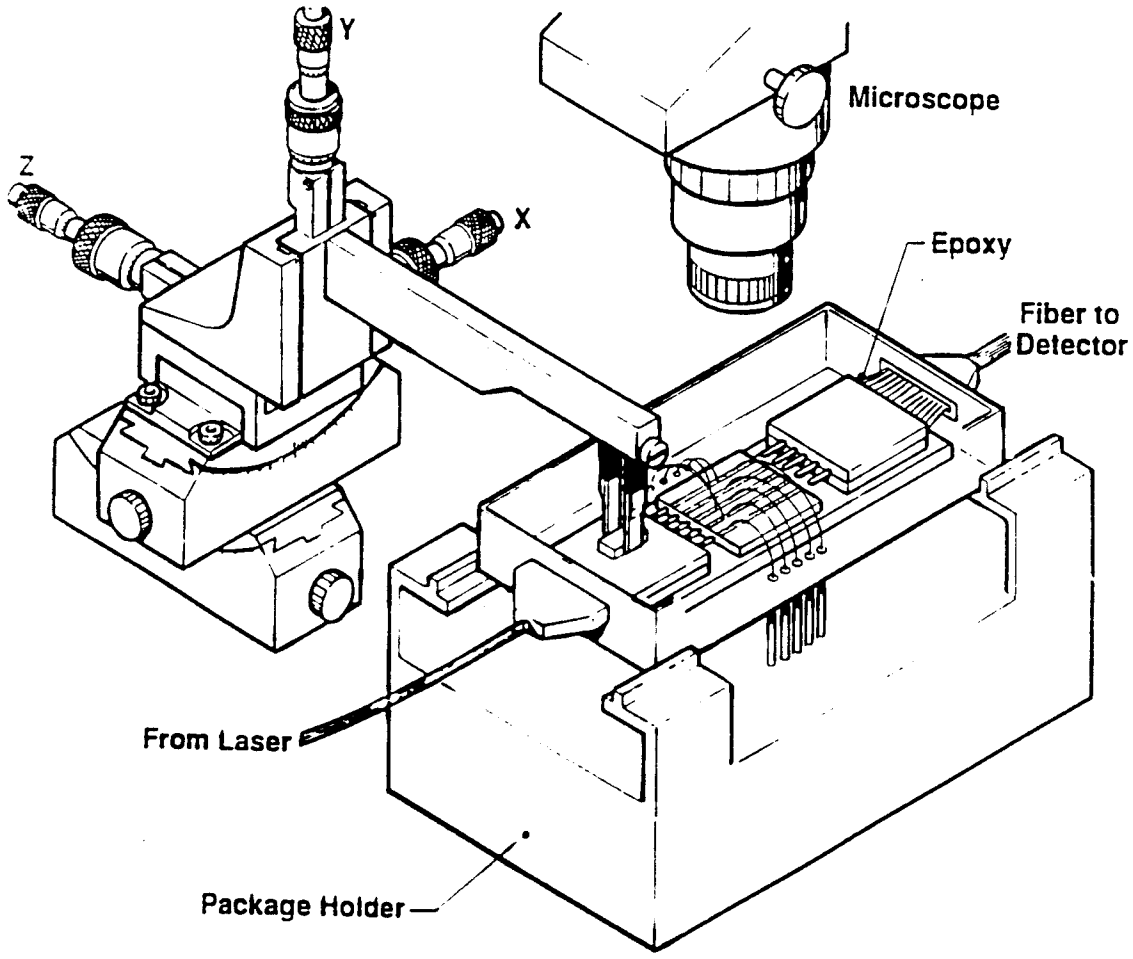

Figure 4-9
Schematic Diagram of the Assembly Equipment

4.8 Soldering

Soldering causes thermal shrinkage of the assembly equipment and the solder volume upon solidification. This is usually unavoidable. If the equipment has a 1m length, a thermal expansion coefficient of 10^{-6}/°C, and a temperature shift of 100°C, there will be a μm order misalignment, which leads to unsuccessful assembly. This misalignment can be canceled in POC's new assembly architecture.

The soldering process developed by POC is shown in Figure 4-8. It uses a new thermal shrinkage compensation method. The point of this method is that the single-mode fiber array block and channel waveguide array block are each held by two pairs of chucks having symmetrical structures and a low thermal expansion coefficient. Further, the chucks and micropositioners are adiabatic from the heater. In the soldering process, two solder layers between the two blocks and the mount are fused by the heater. Thermal shrinkage of the two chuck pairs and the two solder layers arises symmetrically. For the X, Y, θx, θy and θz axes, misalignment on the side of the single-mode fiber array is compensated for by misalignment on the side of channel waveguide array. In this, the single-mode fiber array block and the channel waveguide array block are soldered to a common mount with minimal misalignment.

After soldering, the assembled mount is fixed to the package using solder with a lower melting point. Finally, the package and the cap are hermetically solder-sealed. Because the assembly is performed before sealing the package, no work space is necessary inside the module. Therefore, the module can be made compact and narrow. This compact size is suitable for the use of a large number of modules in a real system. Assembly without adhesives has allowed the modules to have higher reliability at high temperatures.

5.0 DEMONSTRATION OF ALL OPTICAL LOW THRESHOLD GaAs SWITCH

5.1 All-Optical Modulation Setup

A singlemode (8.7 μm core diameter) optical fiber was used to couple a 2.5 mW 1.3 μm laser beam into the GaAs optical switch, as shown in Figures 5-1 and 5-2.

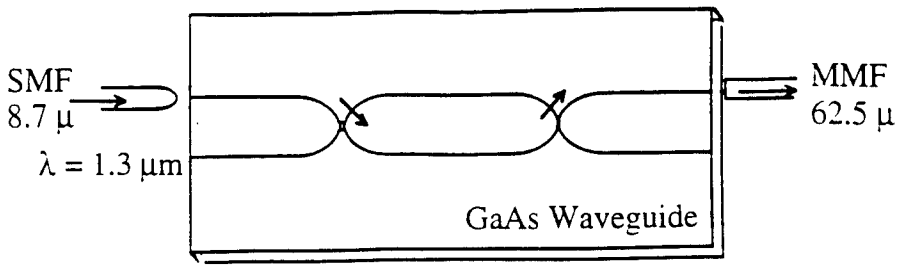

Figure 5-1
8.7 μm Core-Diameter Fiber was Used to Couple 1.3 μm Laser Beam From Semiconductor Laser into the GaAs Optical Switch. At the end of the waveguide, a 62.5 μm core-diameter fiber was used to couple out the laser beam.

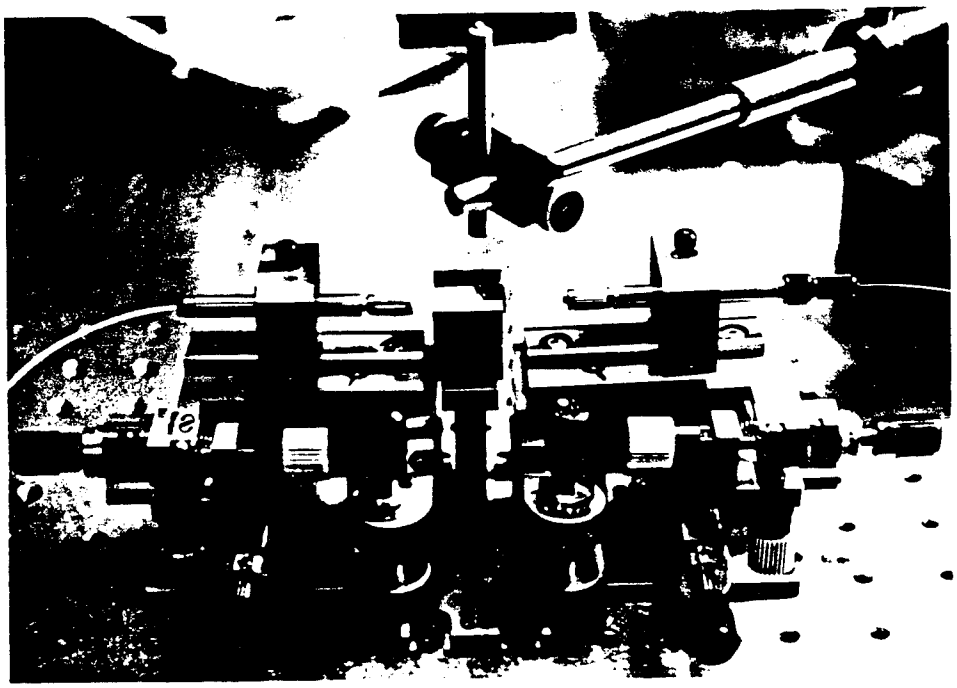

Figure 5-2
1.3 μm Laser Beam was Coupled into the Optical Switch from the Left-Hand-Side Single-Mode Fiber. The switched laser beam was then collected by a multi-mode fiber from the right-hand side. The pumping beam illuminates the X switch from the top.

The output light from the optical switch was then collected by a 62.5 μm multimode fiber. The optical switch was controlled by a laser beam from a Ti:Sapphire laser with an energy higher than the GaAs bandgap. A singlemode fiber was used to couple the laser beam from the Ti:Sapphire laser to the switch. The laser beam illuminated the intersection of the optical switch from the top, as shown in Figure 5-3. In order to observe significant optical switching, the pumping power from the Ti:Sapphire laser should be high. However, if the pumping power is too high, the heating effect will degrade the performance.

The complete setup of the all-optical switch is shown in Figures 5-4 and 5-5.

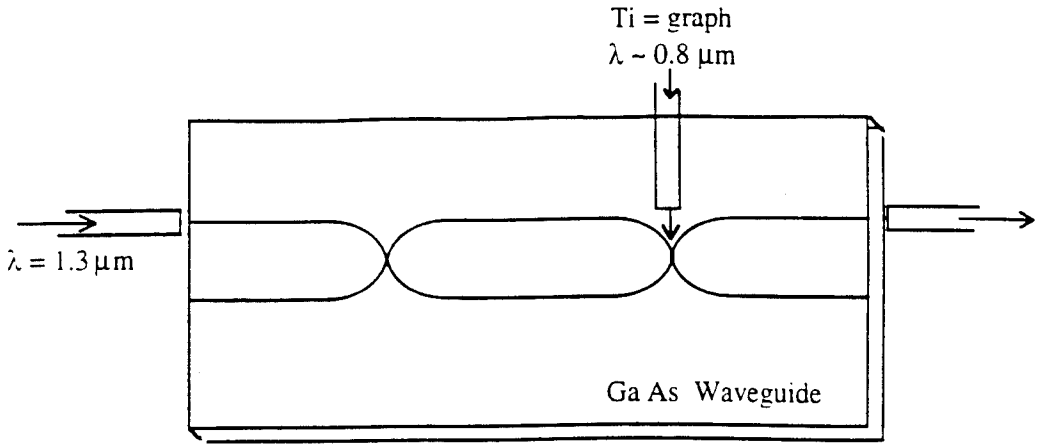

Figure 5-3
Tunable Laser Beam from Ti:Sapphire Laser was Used to Control the 1.3 um Beam Switching. The pumping light energy must be higher than the GaAs bandgap energy.

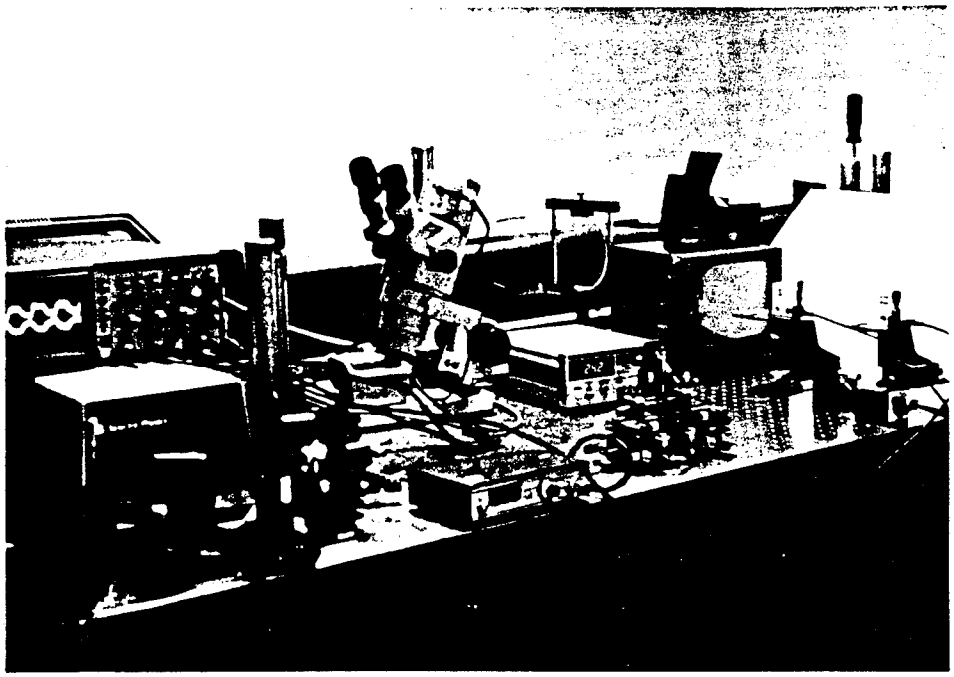

Figure 5-4
Photograph Showing the All-Optical X-Switch Measurement Setup

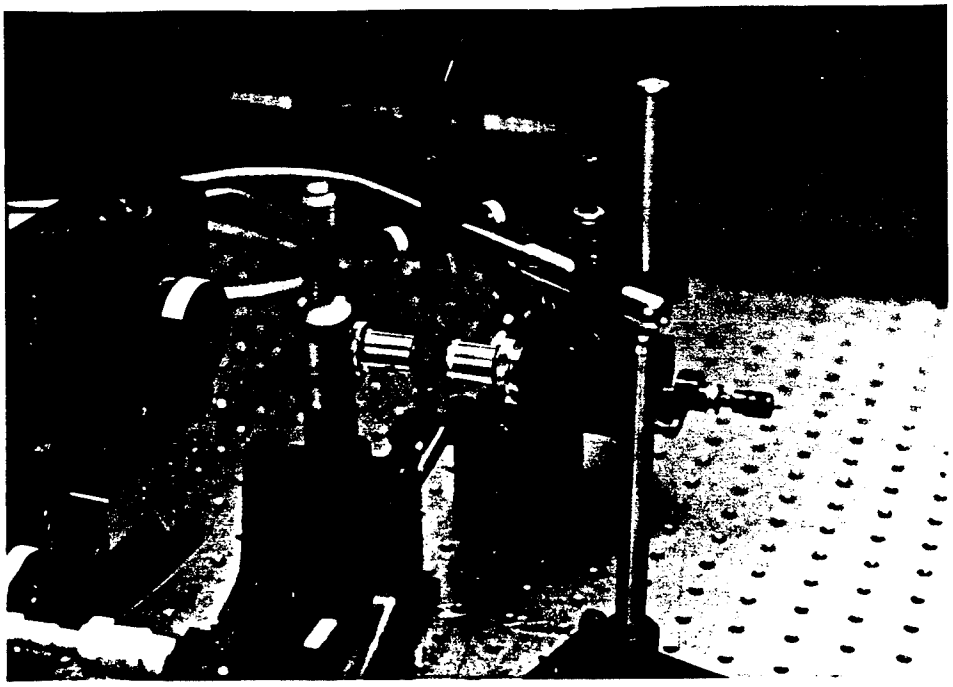

Figure 5-5
Pumping Light is λ = 0.78 µm From Ti:Sapphire Laser

5.2 All-Optical Switch Fabrication

The epistructure of the all-optical switch was grown using the MOCVD method on a GaAs substrate. A 1.5 µm thick undoped $Al_{0.07}Ga_{0.93}As$ cladding layer was first grown on the substrate. Then, a 4 µm undoped GaAs layer was grown on the top as a guiding layer. Conventional photolithography techniques were used to pattern the singlemode optical switches, as shown in Figure 5-6.

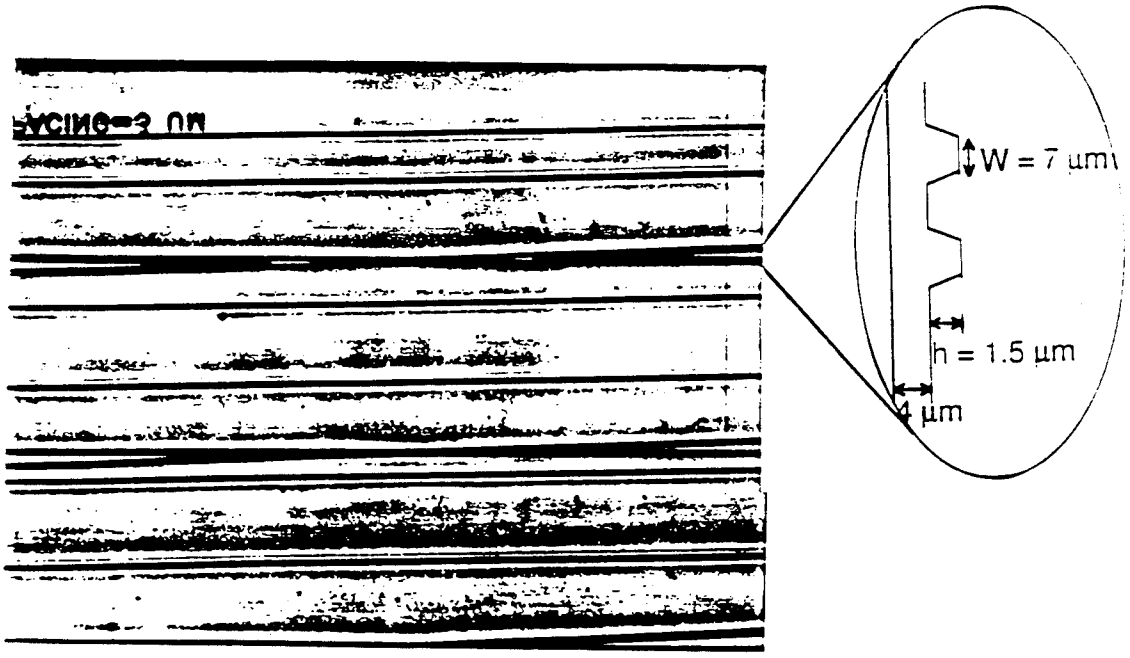

Figure 5-6
Photograph Showing the All-Optical X Switches. The width of the waveguide is 7 µm. The step height is h = 1.5 µm. The guiding layer is 4 µm thick. The pumping beam (λ = 0.78 µm) only illuminates the intersection areas.

5.3 All-Optical Switching Results

The switched laser beam was monitored by two InGaAs PIN detectors. The switched beams were first coupled to the singlemode fibers, and were then detected by the detectors, as shown in Figure 5-7.

The measured responses from the two arms of the X-switch are shown in Figure 5-8. When the pump light was on, the 1.3 µm guided beam was switched to arm (out 1). When it was turned off, the probe beam is switched back to arm (out 2). These results can be observed from the 180° phase change shown on the oscilloscope.

The absorption depth of the pumping light is a function of wavelength. It is well known that higher energy laser beams have shorter penetration depths. But, if the laser beam energy is lower than the GaAs bandgap, no switching will be observed. In order to observe this effect, the Ti:Sapphire laser was tuned from 700 nm to 900 nm. It was seen (see Figure 5-9) that when the pump light energy was below the GaAs bandgap, the modulation depth dropped dramatically. At shorter wavelength ranges, the modulation depth dropped slowly, due to the reduced absorption depth.

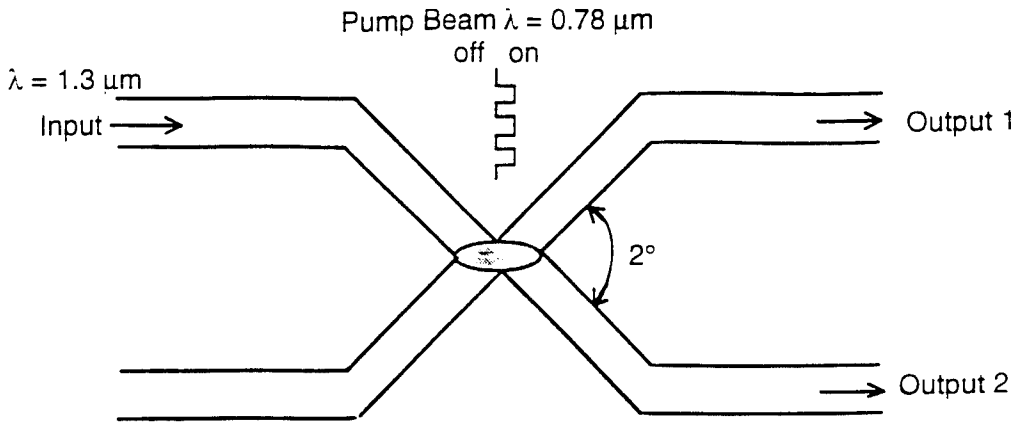

Figure 5-7
Output Signals From Different Arms of the X-Switch were Coupled to the Single-Mode Fibers and Monitored by Two InGaAs PIN Detectors

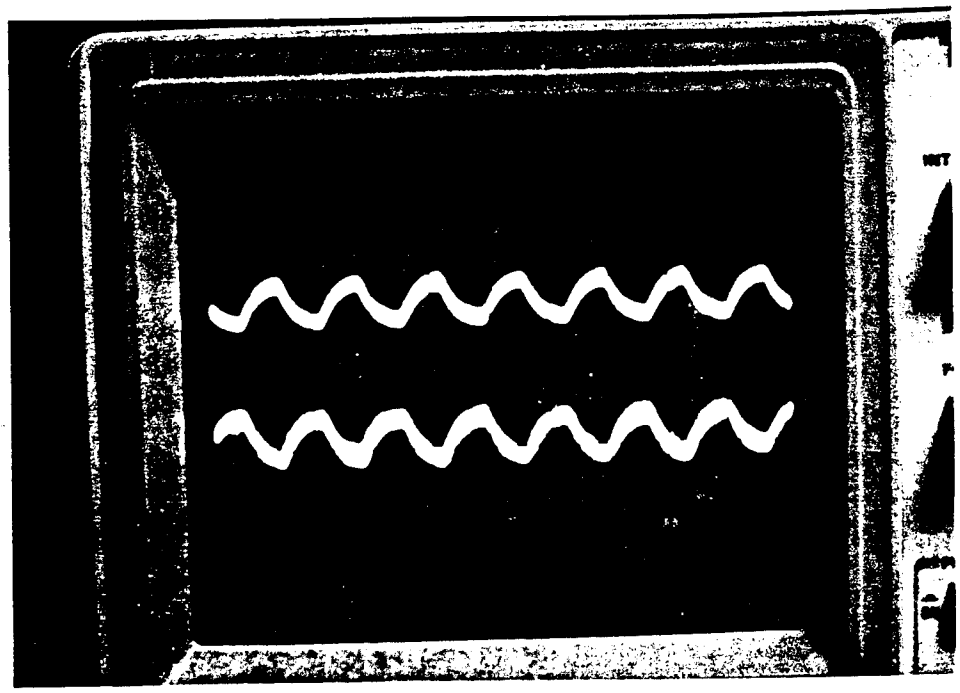

Figure 5-8
Output Signals From Different Arms of the X-Switch. When the pump beam is on, probe beam is switched to arm (out 1). When it is off, the probe beam is switched back to arm (out 2) again.

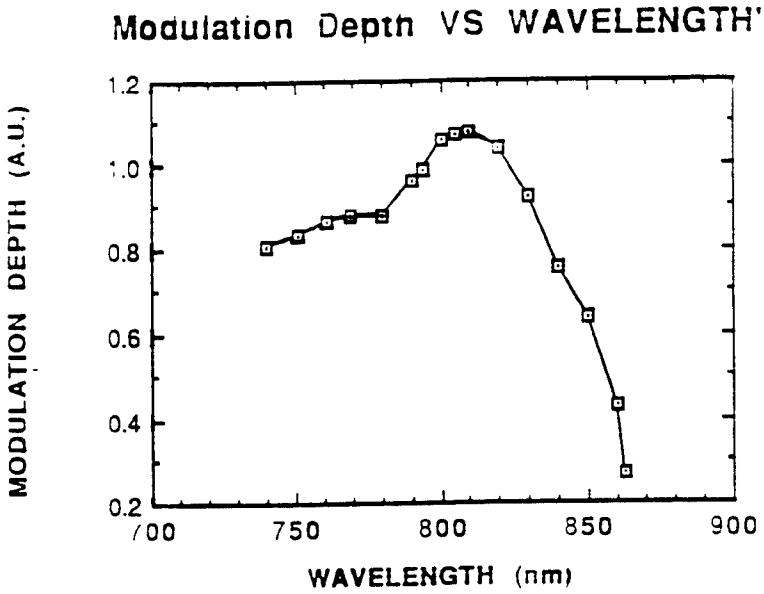

Figure 5-9
Modulation Depth as a Function of Pumping Wavelength. Modulation depth drop dramatically, when the pumping light energy is below the GaAs band gap. Modulation depth drop slowly at short wavelength range, due to the reduced absorption depth.

5.4 The AutoCAD Design of Channel Waveguide Array

in Phase II, POC determined the basic waveguide dimensions and crossbar switch configuration. The parameters of the channel waveguide, such as waveguide width and depth, were also determined. The engineering design of every layer of the crossbar switch can be performed using the AutoCAD software. In order to fabricate complete 10x10 switch, POC designed a 10x10 switch mask, as shown in Figure 5-10. This design will determine the actual size of crossbar switch, which, in turn, provides the whole unit package design.

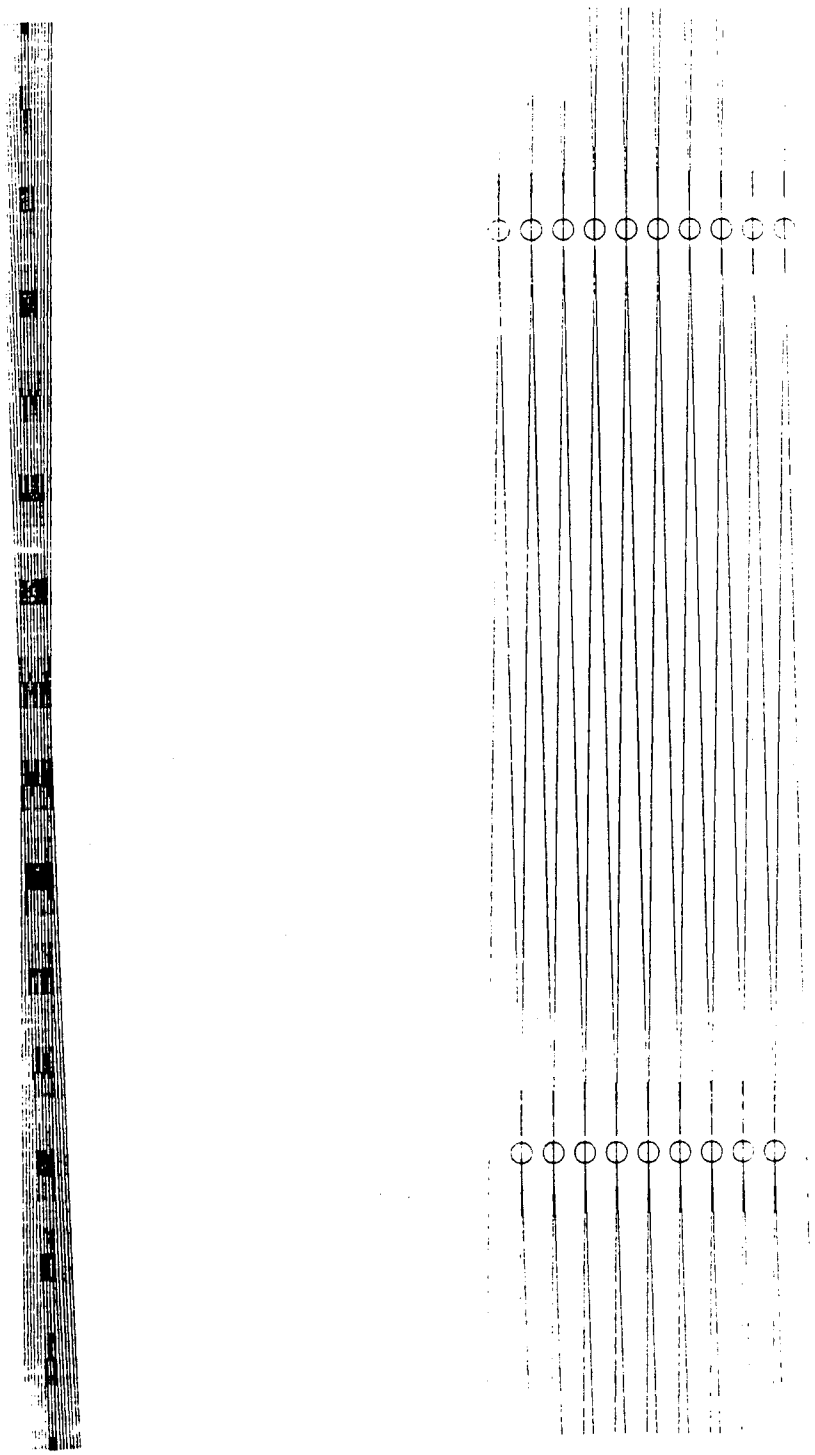

(a) (b)

Figure 5-10
(a) CAD Designed Crossbar Switch Configuration in Scale 1:10; and (b) CAD Designed Crossbar Switch Configuration 1:100. The waveguides separation is 100 μm, the external diameter of fiber core cading is 125 μm.

Using AutoCAD, a 10x10 crossbar switch structure is drawn by first drawing a line from left to right with a one degree angle and another line from right to left intersecting the first line with a 179 degree angle. This creates the required switch structure with a 2 degree intersection angle. The next step is to construct an array realizing 10 of these lines at 125 μm apart. An array of two sets intersecting each other creates 100 intersections. At each intersection, a circle of 125 microns is drawn.

6.0 FUTURE APPLICATIONS

6.1 Optical Switch with Quantum Well Devices

The speed of a GaAs all-optical switch with a bulk-type guiding layer is normally limited by the carrier relaxation time, which is typically longer than a nanosecond. In order to enhance the speed and efficiency of these devices, quantum well devices are implemented for high speed applications. Two different quantum well devices that have the necessary large current controllability and high speed performance are discussed in the following sections. The first is a heterojunction bipolar phototransistor (HBPT) device, while the other is a resonant tunneling double barrier device.

6.1.1 Heterojunction Bipolar Phototransistor (HBPT) Optical Switch

POC's HPBT optical switch, shown in Figure 6-1, has the unique high speed and high sensitivity properties needed for optoelectronic applications. Recently, a current gain of 50,000 was demonstrated for a heterojunction bipolar phototransistor, inducing a photosensitivity of 15,000 A/W. Optical switches with HPBT structures have the following advantages:

- ultrahigh speed (~ picosecond)
- ultrahigh sensitivity
- integration capability with other OEICs
- high current gain

The phototransistor action is achieved through the large emitter-collector current I_{EC}, which is controlled by a small base bias voltage V_{BE}. V_{BE} can be induced by electron-hole pair generation inside the emitter-base and base-collector junctions. This mechanism can be utilized for a high speed phototransistor with an ultrahigh current gain, which can be controlled by a weak optical power. Due to the wide bandgap inside the emitter, a "window effect" can be achieved to enhance the device sensitivity. Due to the base energy barrier, most of the emitter current will be blocked by the barrier. When the base barrier is lowered by either electrical or optical means, the large emitter current is then injected into the collector (the guiding layer).

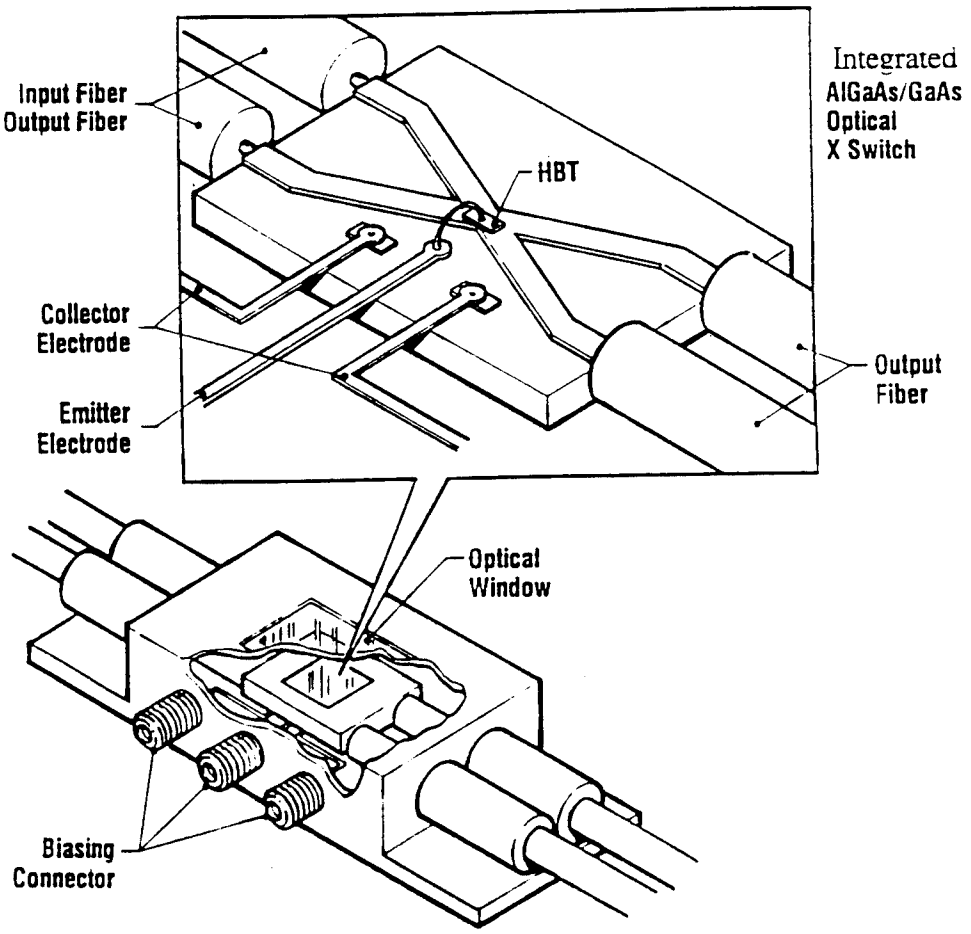

Figure 6-1
POC's High Speed, High Sensitivity All-Optical Switch HBPT Structures

In an HPBT optical switch, only electrons are injected from the emitter into the collector guiding layer, which is not the same as the bulk-type guiding layer that has both electrons and holes generated inside the layer. So, the induced index change, Δn, is expressed as

$$\Delta n = \frac{-2\lambda \Delta N e^2}{m^* n_0 \omega^2} \qquad (6\text{-}1)$$

where m^* is the effective mass of an electron, ω is the frequency, e is the electron charge, n_0 is the intrinsic index of refraction, and ΔN is the injected carrier density.

Several types of optical modulators and switches with p-n junctions whose operations are based on the applications of this phenomenon have been reported. However, the switching time of such diode-structure optical switches is most often limited by the injected carrier life time, which, in

GaAs, is on the order of 10^{-8} s. Due to their high speed and high transconductance characteristics, HBTs are frequently applied in practical transistor circuits for high speed current switching. If a bipolar transistor structure is employed with the carrier injected into the base by optical injection, high speed optical switches and modulators may be achieved. The amplification nature of transistors also means that larger emitter or collector switching currents can be controlled either electrically or optically.

The approximate expressions for the rise time from 0% to 90%, t_r, and the fall time from 100% to 10%, t_f, for the output current when the transistor is driven by a constant input current in the common-based mode are given, respectively,

$$t_r = \left(\frac{1}{\omega_N} + M\alpha_N C_{ct} R_L\right) \ln\left(\frac{I_{E1}}{I_{E1} - \frac{0.9\, I_{Con}}{\alpha_N}}\right) \tag{6-2a}$$

$$t_f = \left(\frac{1}{\omega_N} + M'\alpha_N C_{ct} R_L\right) \ln\left(\frac{I_{Con} + \alpha_N I_{E2}}{0.1 I_{Con} + \alpha_N I_{E2}}\right) \tag{6-2b}$$

where I_{E1} and I_{E2} are the values of the emitter current after the turn-on and turn-off steps are applied and α_N and ω_N are the normal small-signal current gain and cut-off frequency, respectively. I_{Con} is the collector current in the on-state, C_{ct} is the depletion layer capacitance, R_L is the load resistance, and M and M' are the functions of the collector-base voltages and the diffusion potential difference between the collector and base, respectively. The switching times as a function of the input emitter current are shown in Figure 6-2.

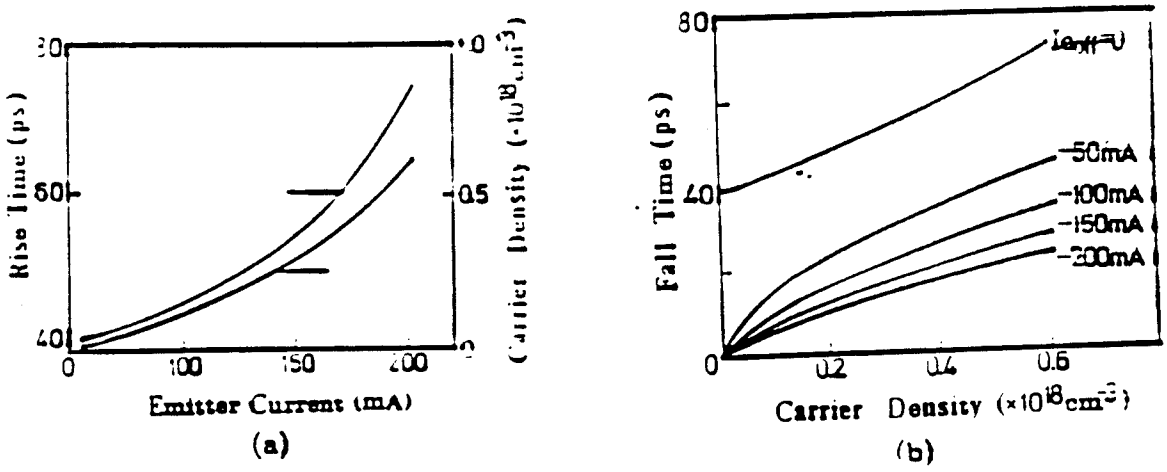

Figure 6-2
Calculated Switching Times of the Transistor: (a) Rise Time t_r and (b) Fall Time t_f

Note that both the rise time and the fall time will be around 50 ps for optical switching. Furthermore, POC's HB phototransistor benefits from the emitter "window effect", which makes it possible to illuminate the active zone through the wide band-gap emitter without the need for over dimensioning of the lateral zone. This is significant, because overdimensioning will sacrifice frequency performance. The other advantage of implementing the HB phototransistor structure within an optical device is the high current gain, which increases the sensitivity of the device and leads to a reduction in the surface area that needs to be illuminated.

6.1.2 Resonant Tunneling Double Barrier Quantum Well Optical Switch

The tunnel diode was named after Esaki, who first discovered it in 1958 [9]. The tunneling phenomenon is a majority carrier effect. Its response time is not limited by the minority carrier recombination lifetime (slow). The tunneling time of carriers through the potential energy barrier is not governed by the conventional transit time concept, but rather by the quantum transition probability per unit of time. This tunneling time is very short, permitting the use of tunnel devices well into the millimeter-wave region [10].

The applications for resonant tunneling diodes, including bistable operation [11], are all based on the negative differential resistance (NDR) in the current-voltage characteristic of the device, as shown in Figure 6-3. Furthermore, the use of a quantum well to form the double barrier structure means better control of the tunneling and the confinement of energy levels at room temperature [12]. The current voltage characteristics of a double barrier resonant tunneling diode shown in Figure 6-3, focuses on the negative differential resistance region. The peak current is primarily determined by the number of electrons passing through the resonant level. Thus, the magnitude of the peak current is influenced by the width of the resonant level. The valley current is the sum of the current contributions, such as non-resonant tunneling, tunneling through excited states in the quantum well, thermionic emission over the barriers, scattering assisted tunneling processes and leakage currents through surface states.

A resonant tunneling diode with a peak current density over 2×10^5 A/cm^2 has been demonstrated [13]. The higher the peak current, the more efficient the modulator/switch will be. Bistable operations of LED's and quantum well semiconductor lasers [14] have already been demonstrated by the integration of a resonant tunneling diode within the device structure. The waveguide modulator/switch will be the next target for state-of-the-art research in integrated optics.

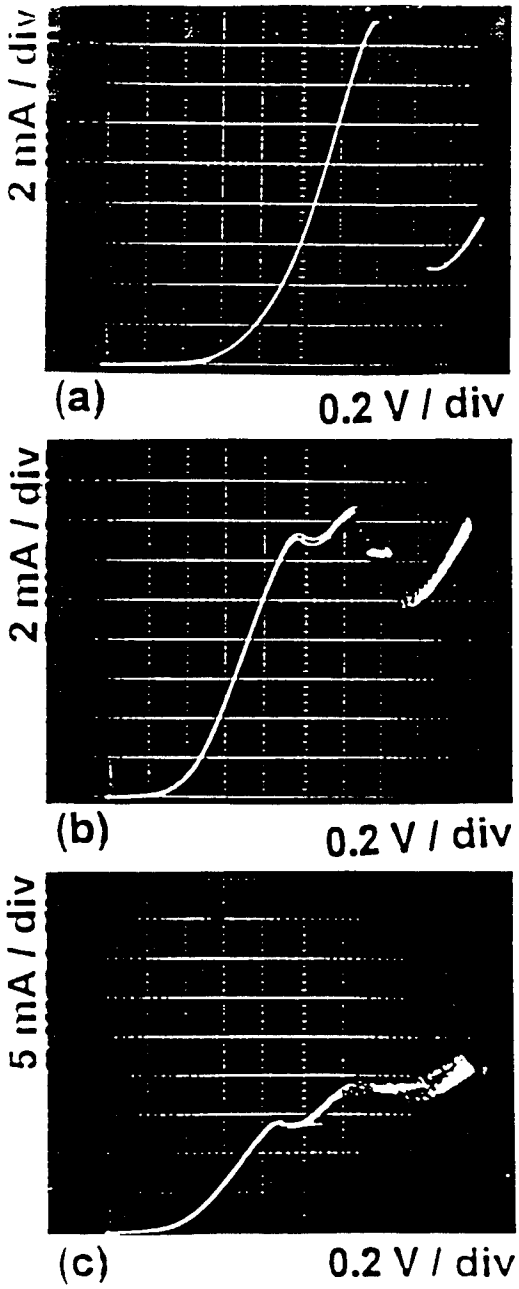

Figure 6-3
I-V Characteristic of Negative Differential Resistance (NDR) in the Resonant Tunneling Diode with Different Illuminating Laser Powers

In this program, Physical Optics Corporation (POC) has proposed a femtosecond optical guided wave switch/modulator integrated with a resonant tunneling double barrier quantum well (RTDBQW) diode. Figure 6-4 demonstrates a variety of integrated optic modulator/switch configurations in combination with RTDBQW structures. The integrated optic waveguide structures that can be used are: (a) a Mach-Zehnder interferometer modulator; (b) a total internal reflection (TIR) switch; (c) a directional coupling modulator; and (d) a cut-off modulator. The current injection mechanism is performed through the highly efficient RTDBQW with low voltage. The speed of this device is not limited by conventional diode transit times, but only by the quantum tunneling time, which is in the *femtosecond regime* [15]. In addition, *due to its inherent negative resistance current-voltage relationship, the device operates in a bistable mode*. This is an extremely important characteristic if the device is to be used as an optical switch in high performance optical computing systems.

In summary, this structure offers efficient current injection, low switching voltage (~ few volts), super high speed (subpicosecond), and bistable operation. Being the basic building block for super high speed (femtosecond) optoelectronic computing and signal processing, this generic concept has the potential to span a broad variety of unique photonic components, including optical logic gates, EO modulators/switches, variable delay lines, and crossbar reconfigurable interconnects.

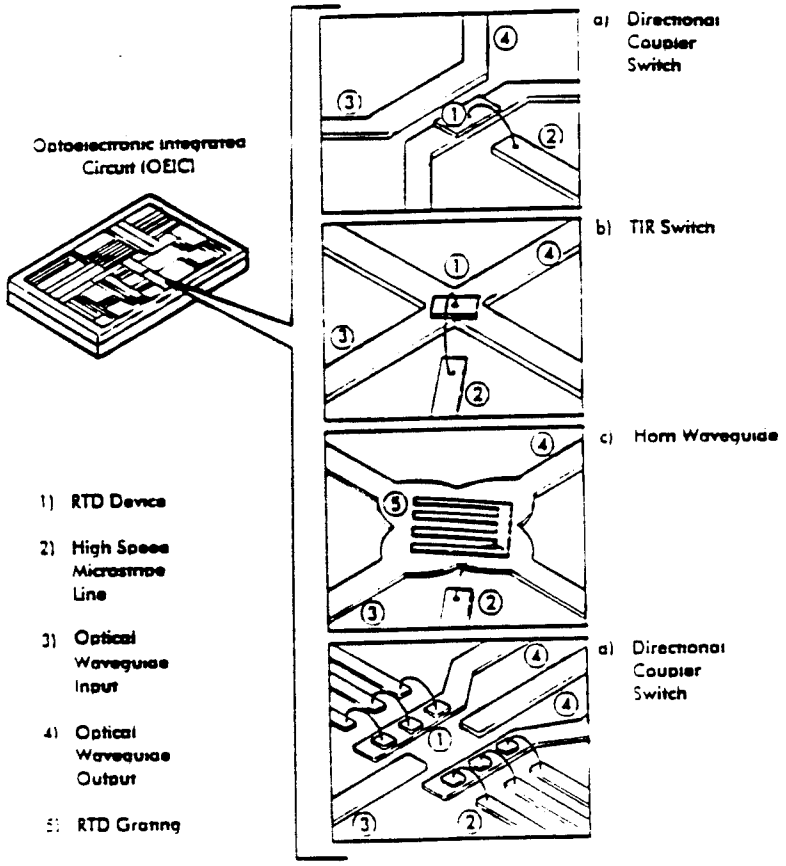

Figure 6-4
POC's Proposed Integrated Modulators/Switches With Resonant Tunneling Double Barrier Quantum Well Diode

6.2 High-Speed Laser Wavelength and Incident Direction Sensors

The proliferation of laser weapons and laser guidance artillery has created a dangerous environment for both military personnel and equipment. Detecting the wavelength and incident direction of laser radiation in a timely manner is a paramount issue in real time strategic defense. The optically activated modulator array working with a holographic band-pass filter plate, which POC has the in-house capability to produce, is an excellent sensor system for application in this area. Figure 6-5 illustrates the concept of such a sensing system. For three-dimensional detection, the three parameters which need to be determined are wavelength, spherical angle θ, and azimuthal angle φ. The holographic band-pass filters associated with the GaAs OAM array have different center wavelengths. The two surfaces for the GaAs OAM array are located in the x-z and y-z planes. For each linear "pixel" p_j, the holographic band-pass filter has a center wavelength Λ_j. The linear arrays of the holographic filters project the incident light onto the two linear pixels of the GaAs OAM such that

$$\lambda \sin\theta \cos\varphi = \Lambda_a \tag{6-3}$$

$$\lambda \cos\theta = \Lambda_b \tag{6-4}$$

and

$$\theta = \tan^{-1}\left(\frac{d_2}{d_1}\right) \tag{6-5}$$

where Λ_a and Λ_b are the holographic rejection bands associated with planes 1 and 2, respectively, and d_1 and d_2 are the projected distances (Figure 6-5). All these parameters can be experimentally determined through the OAM linear arrays. The unknown factors, i.e., λ, θ, and φ, can be automatically determined through Eqs. (6-3) to (6-5). Note that the laser diode arrays and the detector arrays which are located at the input and output faces of the GaAs OAM arrays are not shown. The two linear pixels that are turned on by the incident laser beam can be detected by observing the intensity change of the OAMs through photodetectors.

The range of wavelength detection can be adjusted by choosing an appropriate semiconductor material as the optically activated switching device. The size of each linear pixel is optimized such that low illumination intensity can be detected. For instance, a linear pixel of 5 cm (5 μm x 10^4) should be able to detect incident light in the μW region.

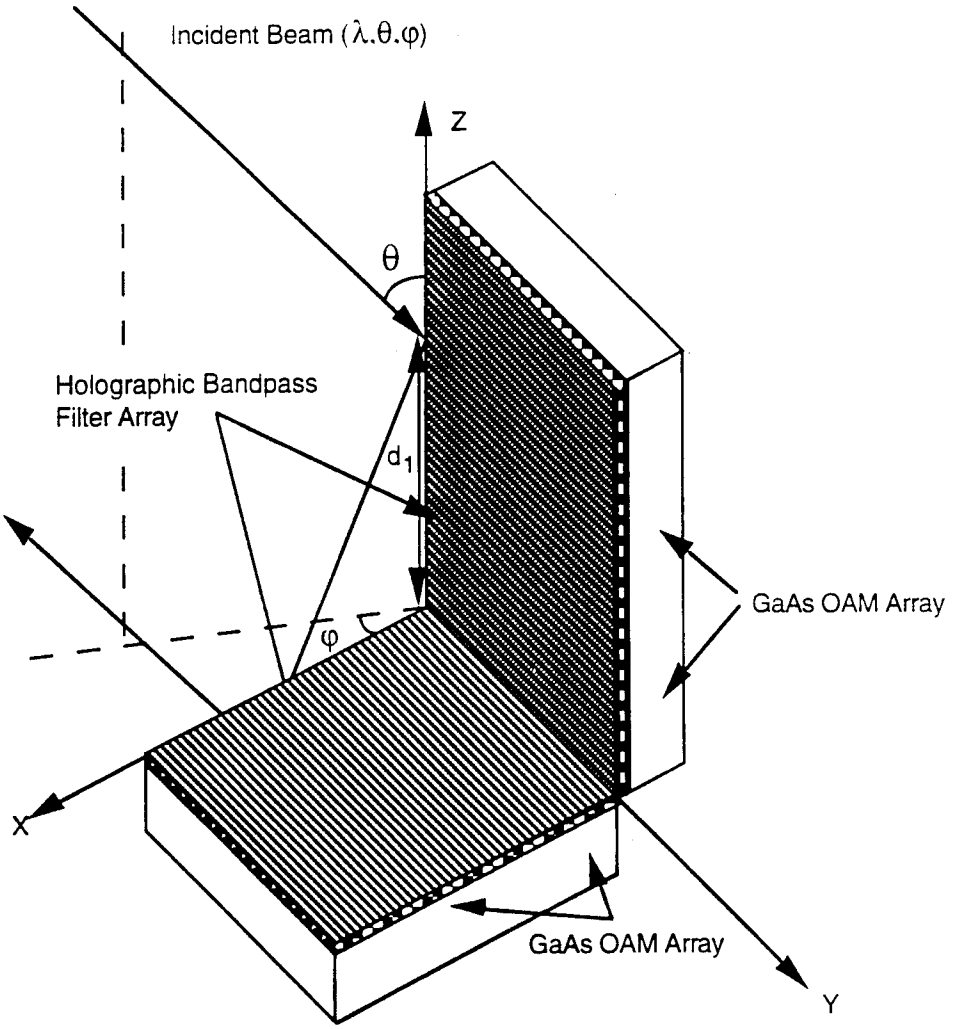

Figure 6-5
High Speed Laser Wavelength and Incident Direction Sensor

6.3 GaAs-OAM-Based IR Countermeasure System

An IR modulator working within the spectral width of 3-to-5 μm can protect military vehicles from heat-seeking missiles. Currently, such modulation is realized by: 1) using an electrical chopper; or 2) directly switching the power line on/off. These methods are not reliable because of the difficulty of changing the modulation speed and the slowness of the switching.

Since GaAs is transparent in these wavelengths, our proposed modulation concept will facilitate the production of an excellent device for this application. The described working principle was used for the basis of the GaAs-OAM-based IR countermeasure system illustrated in Figure 6-6. The modulation speed is equivalent to that of the A-O Bragg cell. Modulation speeds from kHz to GHz can easily be achieved by choosing an appropriate Bragg cell. The diffuser located at the output end is to enlarge the angle of view for the incoming missile.

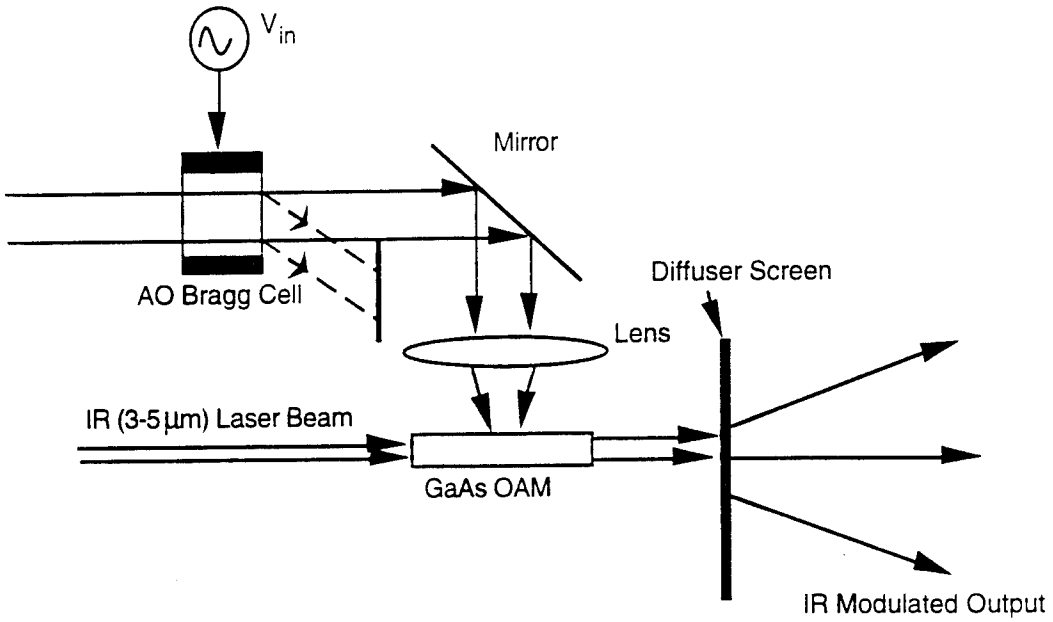

Figure 6-6
GaAs-OAM Based IR Countermeasure System

6.4 Delay Lines for Microwave and Millimeter Wave Phased Arrays

Active microwave and millimeter wave arrays require the distribution of signals over long distances with very precise control of amplitude and phase. The schematic representation of the OAM-based phased array delay line is shown in Figure 6-7. The highly multiplexed waveguide hologram (HMWH) shown in the figure has the capability of providing 1 to N fanout ($N \leq 1000$). The required intensity and phase modulation of each channel can be realized by either optical activation or electrooptic manipulation. The generation of microwave and millimeter waves can be realized by heterodyned optical beams, as achieved at NRL [36] and the Army's Harry Diamond Lab [37]. The major advantage of the device shown in Figure 6-7 is the incorporation of an HMWH with an OAM array to provide a large number of channels. This is not achievable through cascaded systems [38].

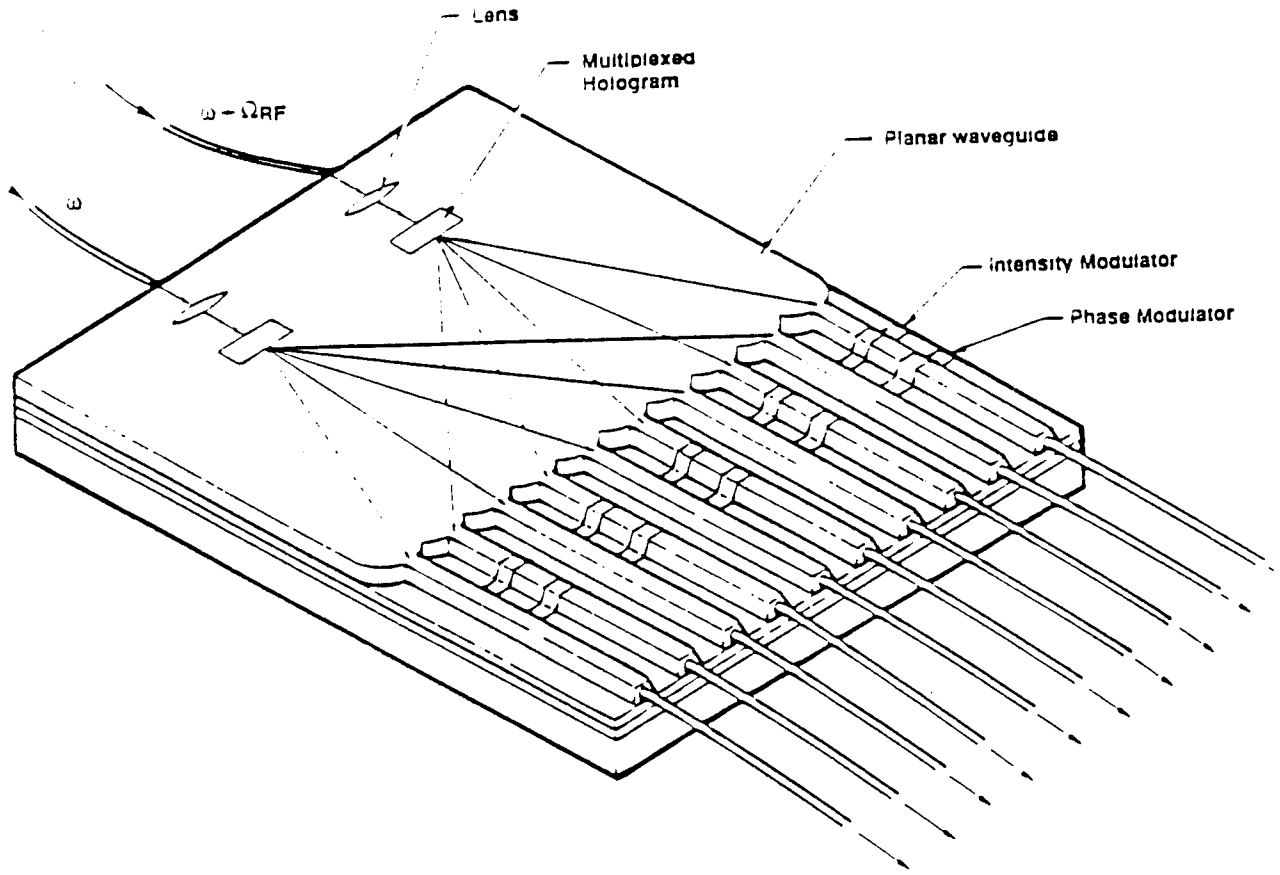

Figure 6-7
Delay Lines for Phased Array Antennae

6.5 Optical Gates

GaAs OAMs working in both the phase- and cutoff-regimes can be used as optical gates. An all-optical OR gate is shown in Figure 6-8. It uses the 0.63 μm optical wave and an electrical signal added through the SMA connectors as the two logic inputs. The optical throughput (1.3 μm IR guided wave) is the logic output. The truth table is also shown. The only condition for the output logic level to shift to 0 is that the 0.63 μm light (A) and the electrical signal (B) are both at the 0 state. Note that the throughput intensity when both A and B equal 1 is higher than for A = 0 and B = 1, and also higher than when A = 1 and B = 0. This discrepancy can be eliminated by setting the threshold level of the photodetector. The realization of an optical NOR gate is easily realized using 0.63 μm light as the input gate signal and a 1.3 μm guided wave as the output gate signal.

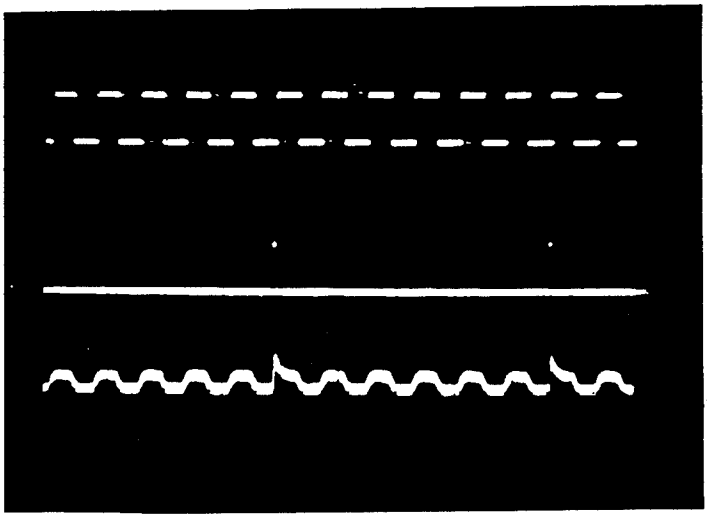

Truth Table

A	0	1	0	1
B	0	0	1	1
C	0	1	1	1

Figure 6-8
Optical OR Gate Using GaAs OAM Working in the Phase Modulation Regime

By biasing an optically activated GaAs cutoff modulator at a suitable reverse voltage and applying the logic inputs at the multiple sections of the Schottky electrode (as depicted in Figure 6-9), NOR, OR, and AND gates [39] are successfully realized. The gate inputs are electrical signals and the gate output is the throughput light of the guided wave. The NOR gate is easily realized by using the input voltage to cut off the throughput light. Whenever the input signal is on ($V \geq V_c$ (cutoff voltage)), the throughput is at minimum intensity, i.e., cutoff, which is defined as 0; otherwise it is 1. The optical OR gate is fulfilled by biasing the device in the cutoff region. Without any input, i.e., A = B = 0 where A and B designate the input signals, the throughput is at a minimum, and therefore, we have Y(output) = 0. However, whenever A = 1 and/or B = 1, the operating point of the modulator of the transfer curve is shifted to a region with significant throughput light. We thus have Y = 1. The result for the OR gate is shown in Figure 6-10. Figures 5-10 (a), (b), and (c) display, respectively, the results with A = 1, B = 0; A = 0, B = 1; and A = B = 1. The discrepancy in the throughput intensity of the Y = 1 state for A = B = 1 and A = 1, B = 0 (or A = 0, B = 1) is due to the different operating points involved. This discrepancy may be removed by setting the proper saturation level of the detector. In the case of the optical AND gate, the device is biased to a region that is well below the cutoff so that only when A = B = 1 will the throughput light become significant.

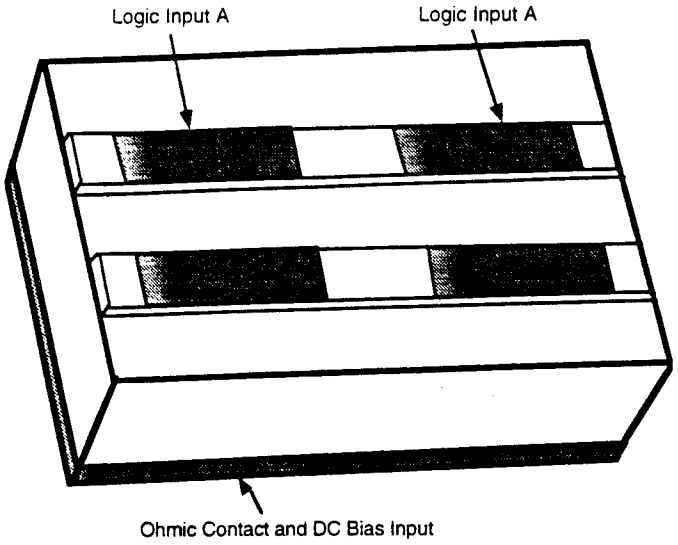

Figure 6-9
Electrode Arrangement for Logic Gate Applications

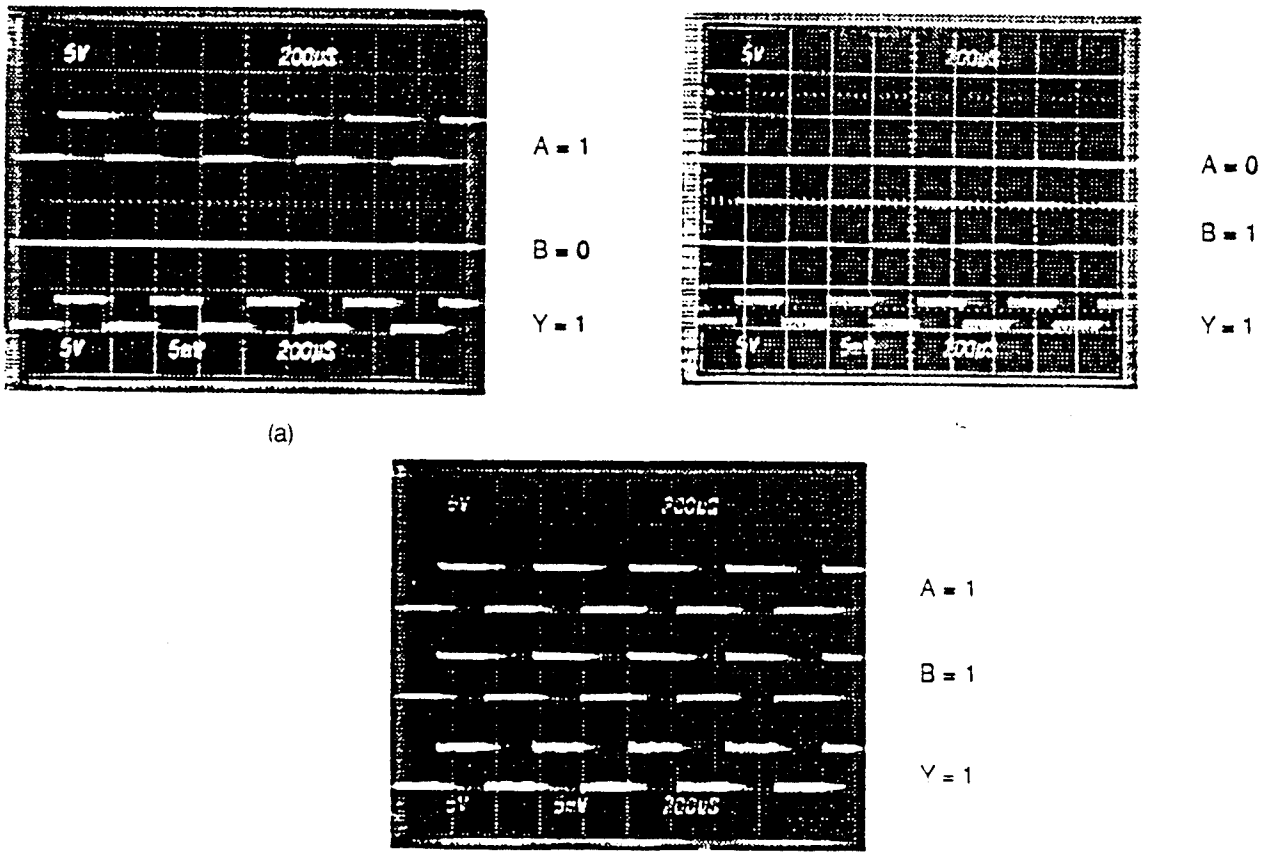

Figure 6-10
The Results Obtained for the Optical OR Gate: (a) A = 1, B = 2, Y = 1; (b) A = 0, B = 1, Y = 0; and (c) A = B = 1, Y = 1. The Result of A = B = 0, Y = 0 is Shown in All Pictures.

6.6 Data Sampling and Encoding, Generation of Very Short Optical Pulses, and Time Division Multiplexing

Optical data sampling is easily realized by applying a DC bias and an RF modulation signal to the GaAs channel waveguide modulator. The laser light coupled into the waveguide is first externally modulated. The data to be sampled is controlled by the proper input sampling signal. The result depends upon the waveform of the sampling signals. Also, when proper gating signals are applied to the multiple modulation electrodes, the modulator can be used to generate a jitter-free train of very short light pulses. These can be used for application in a high-speed sampling oscilloscopes to measure the speed of a fast electrooptic switch/modulator by means of a low speed detector, and to construct an electrooptic sampling system for high frequency optical waveform display.

The approach for generating such short optical pulses follows. Four different microwave signals are individually added to the electrode pads, as shown in Figure 6-11. The frequencies of the input microwave signals are ω, 2ω, 3ω, and 4ω, respectively. If we bias the device in the linear region of the transfer curve of the device, the modulated optical signal due to the combination of these four microwave signals is

$$I_{op} = I_t \cdot \sin(\omega t + \varphi_1) \cdot \sin(2\omega t + \varphi_2) \cdot \sin(3\omega t + \varphi_3) \cdot \sin(4\omega t + \varphi_4) \tag{6-6}$$

where I_t is the throughput intensity without an external AC field, and $\sin(\omega t + \varphi_1)$, $\sin(2\omega t + \varphi_2)$, $\sin(3\omega t + \varphi_3)$, and $\sin(4\omega t + \varphi_4)$ are microwave signals applied to four different electrode pads of the same optical channel. φ_1, φ_2, φ_3, and φ_4 are the delay times, which include the transmit time delay of the guided wave and the microwave propagation delay. The desired delay times can be adjusted through the selection of proper length coaxial cables, or by using line stretchers. The proper delay time is chosen such that

$$\varphi_1 = \varphi_2 = \varphi_3 = \varphi_4 = \pi/2 \tag{6-7}$$

Under this condition, the modulated optical output intensity can be easily derived through simple calculation. The result is,

$$I_{op} = I_t \bullet 64\,[\cos(\omega t)]^{10} \tag{6-8}$$

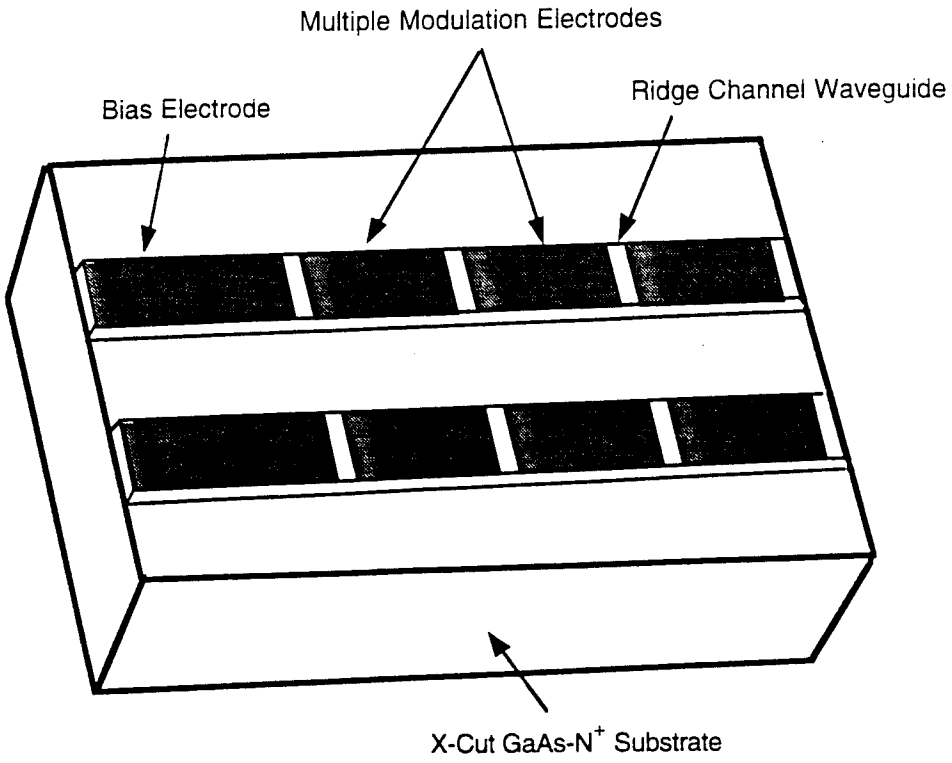

Figure 6-11
Electrode Arrangement for Multiple-Channel Applications of the
GaAs-GaAlAs Heterostructure Cutoff Modulator Array

The output in this condition is the tenth power of cos (ωt). To clarify the condition, a computer simulated optical output and the fundamental mode of the microwave input signal are both shown in Figure 6-12. A very sharp pulse can be generated using this method. If the fundamental frequency of the microwave signal is ω = 1 GHz, an optical pulse with ~100 picosecond 3 dB pulse width can be generated. An even shorter optical pulse can be generated with a higher fundamental microwave frequency. The relationship of the fundamental microwave frequency and the 3 dB optical pulse width is depicted in Figure 6-13. The desired output optical pulse width can be acquired by injecting suitable combinations of microwave signals.

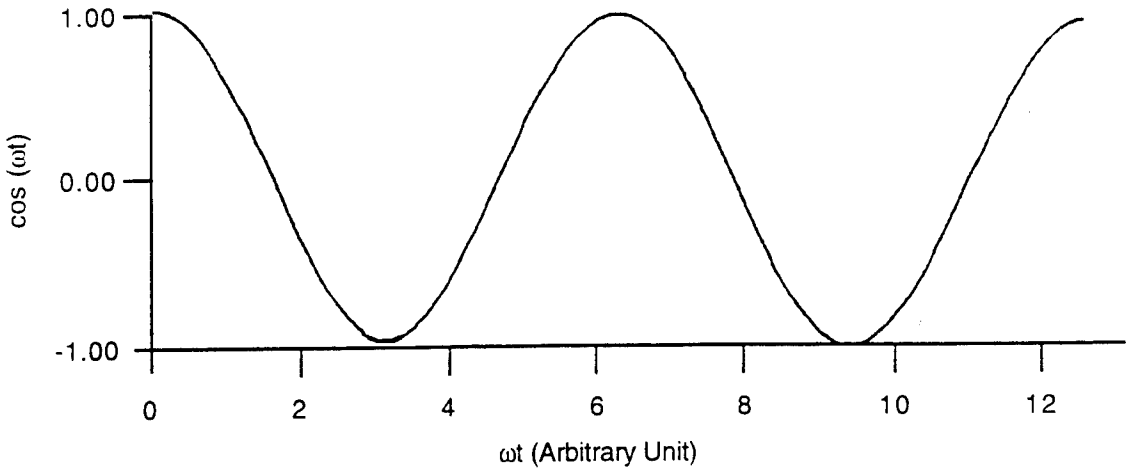

(a)

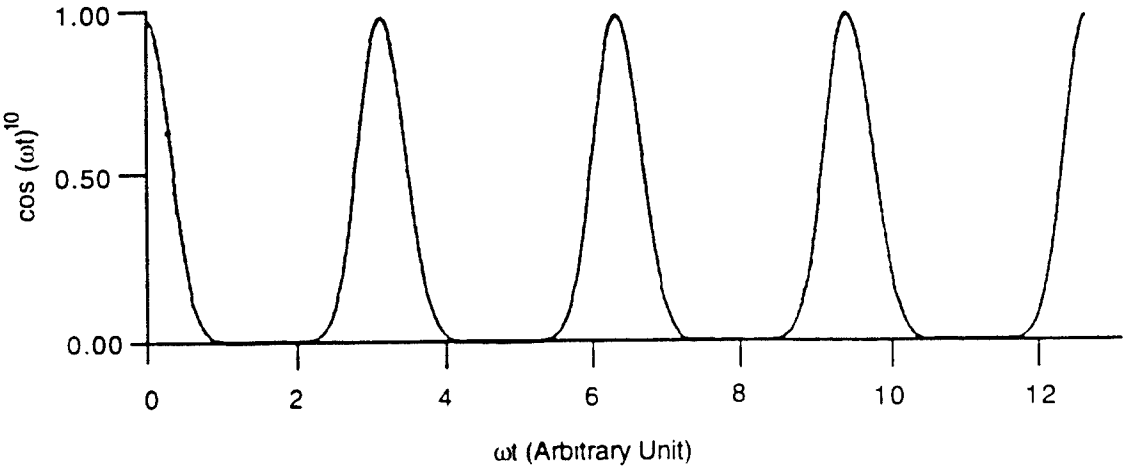

(b)

Figure 6-12
The Calculated Results of the Jitter-Free Optical Pulse: (a) Fundamental Mode cos (ωt) and (b) the Generated Optical Pulses (cos $(\omega t)^{10}$)

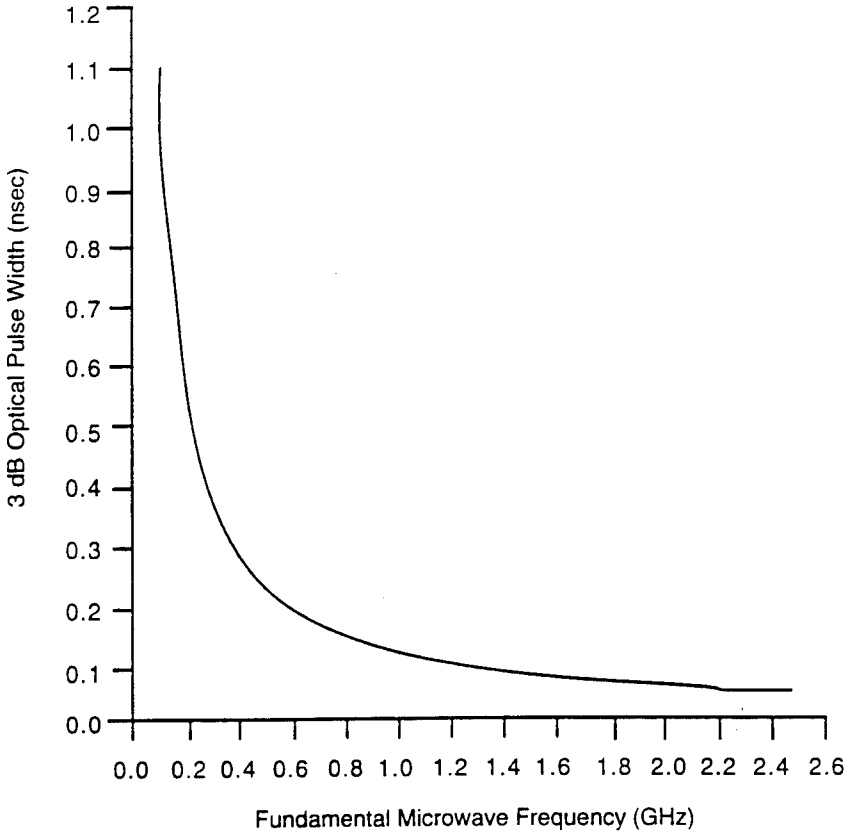

Figure 6-13
Calculated Pulse Width as a Function of Fundamental Mode Microwave Frequency

The encoding and time-division multiplexing (TDM) of multi-channel signals on an optical wave can also be accomplished by applying the signals to multiple sections of the modulating electrode formed on a single ridge channel waveguide (see Figure 6-11). Time-division multiplexing of four channels using a modulator with four electrode sections, each 1 mm long, has been carried out. Figure 5-14 shows the multiplexed waveform of two, three and four channels each with a 10 ns pulse train. The time delays of each pulse sequence are adjusted externally. Clearly, the number of channels to be multiplexed can be greatly increased by utilizing the modulator array together with a waveguide lens fabricated in the same GaAs substrate. Note that GaAs OAMs working in the phase- and cutoff-regimes are both useful for TDM application. However, it should be emphasized that the GaAs optically activated cutoff modulators presented in this section can utilize both coherent and incoherent light sources in all of the applications referred to above. Demultiplexing of the TDM signals can be realized by utilizing the OAM device shown in Figure 6-15 at the receiving port.

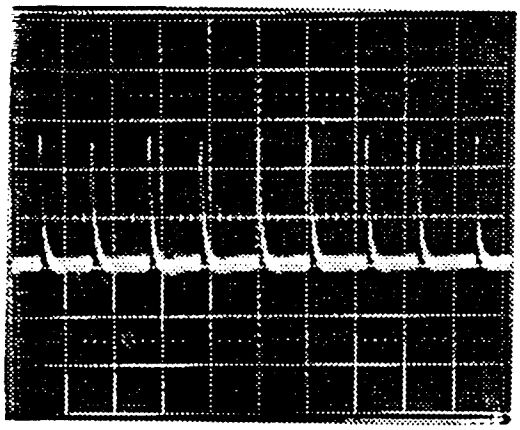

(a)

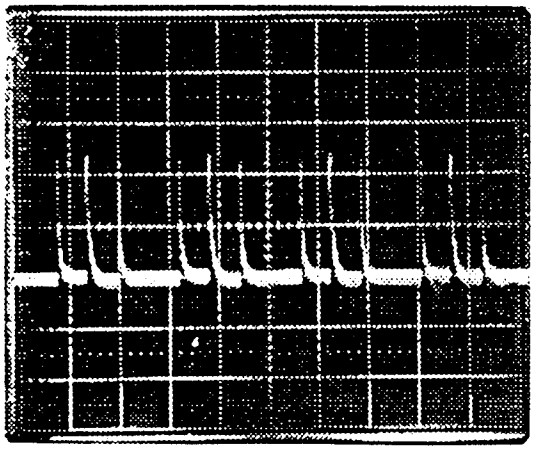

(b)

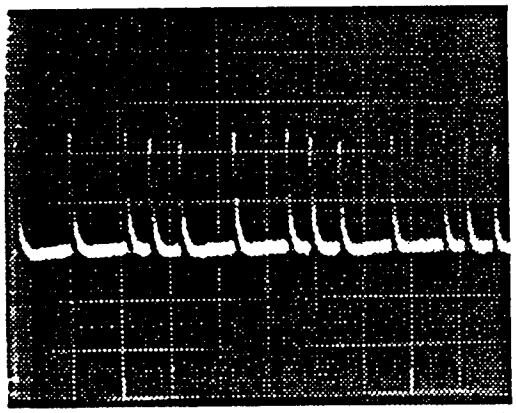

(c)

Figure 6-14
The Multiplexing of Multi-Electrical Pulse Trains: (a) Two Pulse Trains, (b) Three Pulse Trains, and (c) Four Pulse Trains. The Pulse Width is 10 nsec.

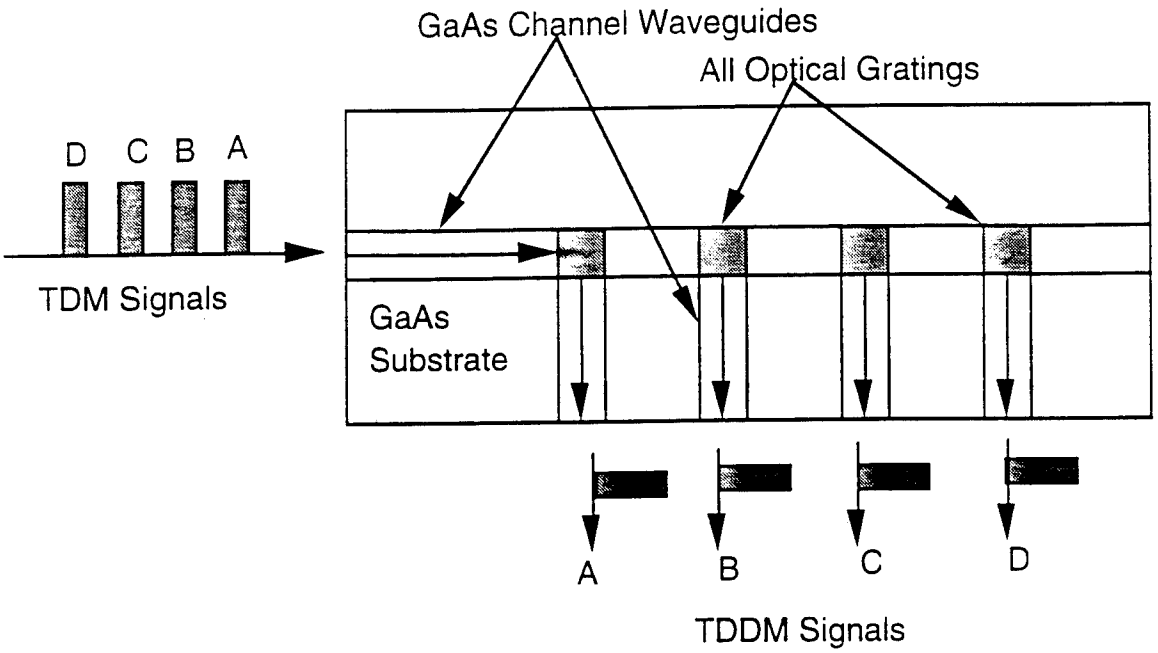

Figure 6-15
Demultiplexing of TDM Signals Using the OAM

6.7 The BER Setup

The ability to switch light gives a unique opportunity to provide very high speed BER measurements at the front-end of communications equipment. Due to the unique nature of optical components (Terahertz bandwidth), many existing metrological problems in high speed measurements can be solved.

The novel BER measurement system shown in Figure 6-16 is able to determine errors at > 100 Gb/s bit data rates. The BER measurement principle is based on the analysis of the reference word, which is formed by sampling every of $2^n \cdot T$ position of the incoming optical data stream [17], where n = 1,2 ... and T is the time slot duration. If we have prior knowledge of the analyzed word structure, we can determine the structure of one n realization and determine the BER performance. Because the repetition rate of the optical pulses in band B is relatively low, we can detect pulses using a low speed opto-electrical integrator and analyze the signal using low speed BER measurement methods. This novel BER measurement setup will solve the metrology problems of existing very high speed (> 10 Gb/s) data links.

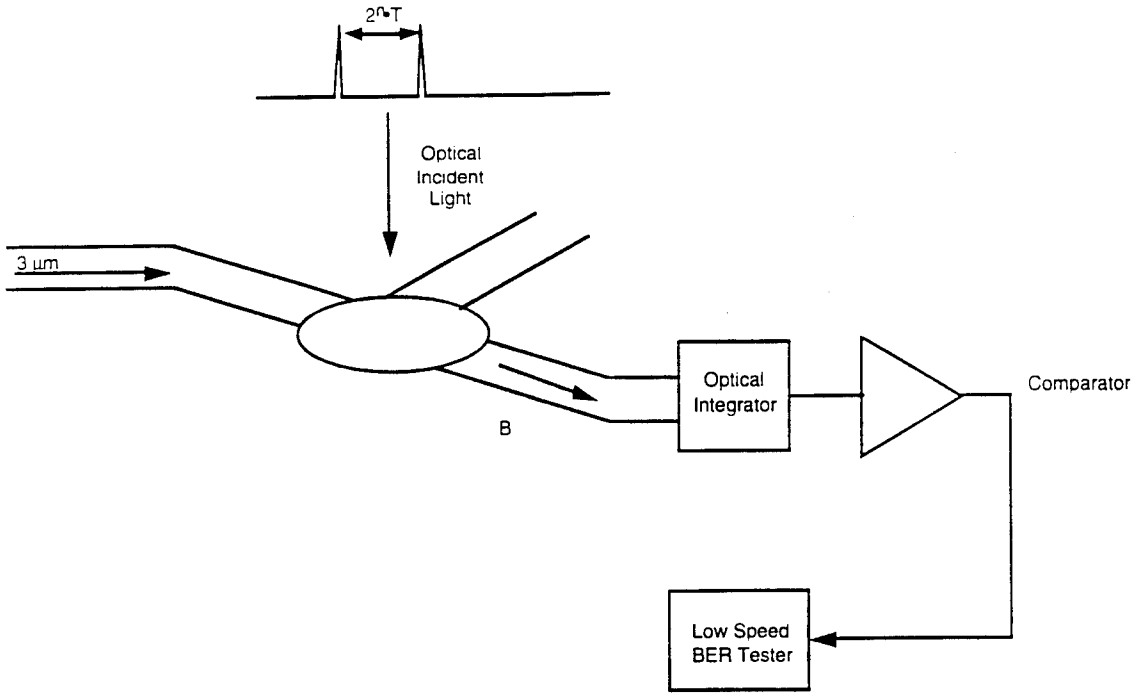

Figure 6-16
The Novel BER Measurement System Utilizing the Properties of a Fully Optical GaAs Switch

6.8 The Evaluation of Nonlinear Distortion

The coefficient of nonlinear distortion (CND) can be defined as

$$CND = 20 \lg \frac{A_1}{A_n} \qquad (6\text{-}9)$$

where A_1 is the first tone amplitude, A_n is the n tone amplitude, and n = 2,3,4 ....

The architecture of the nonlinear distortion measurement system is shown in Figure 6-17. A sine wave generator (HP 8643A) generates a sine wave at a frequency of 10 MHz. This signal is reconverted into the optical domain (1.3 μm wavelength, 0 dB single mode optical output) using the Anaritsu stabilized light source MG 9001A. This stabilized light source is specified for use in a frequency range from DC to 30 MHz. The light coming through the singlemode fiber is coupled into the waveguide (point A) and passed through the switch. If the pump beam is not present, the optical path is AC; the optical path is AB when the pump light is present. By the measuring the optical power at points B and C, we can determine the insertion loss. A power meter is used to determine the output power. In our experiments, the output power measured at points B and C was -6.7 dB and -6.8 dB, respectively. The optical signal (from -6.7 to -6.8 dB levels) is then reconverted from the optical into the electrical domain using an Anaritsu MP 9653 wave monitor, which has a conversion efficiency of > 40 mV/mW. The output signal spectrum is determined

using an HP 8560E spectrum analyzer. The nonlinear second tone distortion was determined to be on the level of -65 dB (20 MHz), and the third tone on the level of < -75 dB (30 MHz). Assuming an optical receiver sensitivity of -35 dB, we can determine the number of optical paths needed to receive the output optical signal, which will be dependent on the sensitivity of optical receiver. In case of an OC-12 system, the number of optical paths cannot exceed 5.

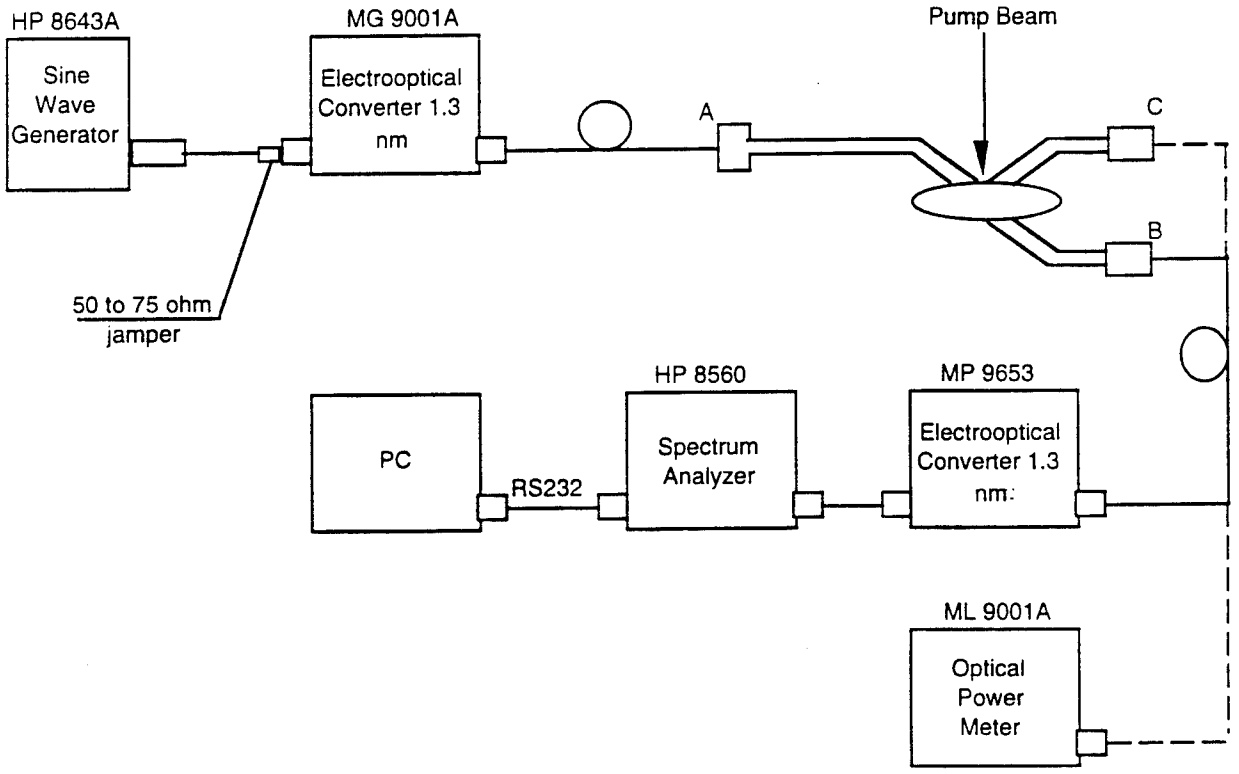

Figure 6-17
The Testbed for Nonlinear Distortion Measurement. First optical path (pump beam is turned off) includes a sine wave generator, an E/O converter, an AC optical path, an O/E converter, and a spectrum analyzer. The second optical path (pump beam is turned on) includes a sine wave generator, an E/O converter, an optical path, an O/E converter, and a spectrum analyzer.

7.0 CONCLUSIONS AND RECOMMENDATIONS

In this Phase II program, Physical Optics Corporation (POC) proposed to develop the basic principles for the fabrication of all-optical crossbar switches. During this program, POC successfully demonstrated the technical, engineering, and theoretical feasibility (including computer modeling and simulation) of POC's new GaAs-GaAlAs crossbar switch concept. The entire project had three major stages:

1. The modeling and computer simulation of highly parallel singlemode channel waveguide arrays.

2. The design, fabrication and packaging of the optical crossbar switch.
3. The demonstration and testing of an all-optical low threshold GaAs switch.

In this program, POC successfully fabricated a 2x2 GaAs/AlGaAs switch that changes the direction of incident light with minimum insertion loss and nonlinear distortion. This unique technology can be used for both analog and digital networks. Because an all optical network does not have any speed limitations (RC time constants), POC's approach will be beneficial for multigigabit and terabit SONET networks, phased array radar networks, very high speed optical sampling scope techniques, BER test equipment, and the rapidly growing video conferencing network market. POC's all-optical crossbar switch will be a key component in the widely proposed all-optical 200 Gb/s. Phase III commercialization will focus on the two principal areas that were investigated in Phase II. One will be multigigabit SONET/ATM networks, while the other will be the multigigabit video conferencing networks. POC will design and fabricate system architectures applicable to both proposed approaches. The material characteristics, switch mask, and fabrication technology will be optimized.

The Phase III efforts will also focus on the application of the all-optical crossbar switch to both the military and civilian sectors. POC will investigate the possibility of using commercial off-the-shelf technologies for the production and manufacturing of the all-optical crossbar switch. Based on our successful track record in the commercialization of products resulting from SBIR funding, POC is confident that its management and technical expertise will continue to result in successful technology development and Phase III transfer to production. Thus far, POC has successfully commercialized the five products:

1. Raman holographic edge filters;
2. Multimode wavelength division multiplexers (WDM);
3. Fiber optic connectors (FOC);
4. Holographic diffusers; and
5. Video and digital data links for multimedia communications.

All of these five products are examples of successful SBIR Phase II and Phase III commercialization efforts. In addition to the government programs, POC collaborates with numerous corporations in the private sector, such as AMP, Monsanto, Boeing, SIV, Melles Griot, Cohu, and others to support existing commercialization and future development through joint venture and licensing agreements. In addition to the above, POC's commitment to commercialization is evidenced by venture capital funding of $2.6 million, which was obtained by our company for the commercialization of products resulting from Phase II SBIR programs.

8.0 REFERENCES

1. R. Chen, "An Optically Activated Modulator and GaAs-GaAlAs Compound Semiconductor Channel Waveguide," Final Report to SDIO, Contract No. F49620-90-C-0068 (1992).

2. R. A. Soref and B. R. Bennett, "Electro-Optic Effects in Silicon," IEEE J. of Quantum Electron., QE-23, 123 (1987).

3. J. P. Lorenzo and R. A. Soref, "1.3 mm Electro-Optic Silicon Switch," Appl. Phys. Lett., 51, 6 (1987).

4. N. K. Dutta, N. A. Olsson, and W. T. Tsang, "Carrier Induced Refractive Index Change in AlGaAs Quantum Well Lasers," Appl. Phys. Lett., 45, 836 (1984).

5. J. Manning, R. Olshansky, and C. B. Su, "Strong Influence of Nonlinear Gain on Spectral and Dynamic Characteristics of InGaAsP Laser," Electron. Lett., 21, 496 (1985).

6. O. Mikami and H. Nakagome, "Waveguide Optical Switch in InGaAs/InP Using Free-Carrier Plasma Dispersion," Electron. Lett., 20, 228 (1984).

7. K. Ishida, H. Nakamura, R. Matsumura, T. Kadoi, and H. Inoue, "InGaAsP/InP Optical Switches Using Carrier Induced Refractive Index Change," Appl. Phys. Lett., 50, 141 (1987).

8. N. W. Ashcroft et al., Solid State Physics (Cornell University, Ithaca, NY, 1976).

9. R. Tsu and L. Esaki, Appl. Phys. Lett., 22 562 (1975).

10. T. C. L. G. Sollner, W. D. Goodhue, P. E. Tannenwald, C. D. Park, and D. D. Peck, IEEE Trans. Electron Devices, ED-30, 1577 (1983).

11. A. Zaslavsky, V. J. Goldman, and D. C. Tasui, "Resonant Tunneling and Intrinsic Bistability in Asymmetric Double-Barrier Heterostructure," Appl. Phys. Lett., 53, 1408 (1988).

12. T. P. E. Broekaert, W. Lee, and C. G. Gunstad, "Pseudomorphic $In_{0.53}Ga_{0.47}$ As/AlAs/InAs Resonant Tunneling Diodes with Peak-to-Valley Current Ratios of 30 at Room Temperature," Appl. Phys. Lett., 53, 1545 (1988).

13. E. Wolak, E. Özbay, B. G. Park, K. Diamond, D. M. Bloom, and J. Harris, "The Design of GaAs/AlAs Resonant Tunneling Diodes with Peak Current Densities Over 2×10^5 A/cm^2," J. Appl. Phys, 69 3345 (1991).

14. I. Grive, S. C. Kan, G. Griffel, S. W. Wu, A. Sa'ar, and A. Yariv, "Monolithic Integration of a Resonant Tunneling Diode and a Quantum Well Semiconductor Laser," Appl. Phys. Lett., 58 110 (1991).

15. J. F. Whitaker and G. A Mourou, "Picosecond Switching Time Measurement of a Resonant Tunneling Diode," Appl. Phys. Lett., 53 385 (1977).

16. A.E.J. Marcatili, "Dielectric Rectangular Waveguide and Directional Coupler for Integrated Optics," Bell Sys. Tech. J., 48, 2071 (1969).

17. V. Katsman, "Adaptive BER Measurement System for very High Speed Communication," Vilnius, Lithuania, p.170. (1986).